Experimental Investigation of the Effect of Surface Markings on the Mechanical Integrity of Weathering Bridge Steels

Final Report

FDOT Contract Number: BDV31-977-02

University of Florida
Department of Materials Science and Engineering
Principal Investigator: Associate Professor Michele V. Manuel
Postdoctoral Researcher: Michael S. Kesler, Ph.D.
Consultant Engineer: Edward George, C.W.I., P.E.
November 21, 2014

The opinions, findings, and conclusions expressed in this publication are those of the authors and not necessarily those of the State of Florida Department of Transportation.

CONVERSIONS TO SI UNITS

SYMBOL	WHEN YOU KNOW	MULTIPLY BY	TO FIND	SYMBOL
LENGTH				
in	inches	25.4	millimeters	mm
ft	feet	0.305	meters	m
yd	yards	0.914	meters	m

SYMBOL	WHEN YOU KNOW	MULTIPLY BY	TO FIND	SYMBOL
AREA				
in^2	square inches	645.2	square millimeters	mm^2

SYMBOL	WHEN YOU KNOW	MULTIPLY BY	TO FIND	SYMBOL
MASS				
lb	pounds	0.454	kilograms	kg

SYMBOL	WHEN YOU KNOW	MULTIPLY BY	TO FIND	SYMBOL
TEMPERATURE (exact degrees)				
^oF	Fahrenheit	5 (F-32)/9 or (F-32)/1.8	Celsius	^oC

SYMBOL	WHEN YOU KNOW	MULTIPLY BY	TO FIND	SYMBOL
FORCE and PRESSURE or STRESS				
lbf	poundforce	4.45	newtons	N
lbf/in^2	poundforce per square inch	6.89	kilopascals	kPa

APPROXIMATE CONVERSIONS TO SI UNITS

SYMBOL	WHEN YOU KNOW	MULTIPLY BY	TO FIND	SYMBOL
LENGTH				
mm	millimeters	0.039	inches	in
m	meters	3.28	feet	ft

SYMBOL	WHEN YOU KNOW	MULTIPLY BY	TO FIND	SYMBOL
AREA				
mm^2	square millimeters	0.0016	square inches	in^2
m^2	square meters	10.764	square feet	ft^2

SYMBOL	WHEN YOU KNOW	MULTIPLY BY	TO FIND	SYMBOL
MASS				
g	grams	0.035	ounces	oz
kg	kilograms	2.202	pounds	lb

*SI is the symbol for the International System of Units. Appropriate rounding should be made to comply with Section 4 of ASTM E380. (Revised March 2003)

1. Report No.	2. Government Accession No.	3. Recipient's Catalog No.

4. Title and Subtitle	5. Report Date
Experimental Investigation of the Effect of Surface Markings on the Mechanical Integrity of Weathering Bridge Steels	November 21, 2014
	6. Performing Organization Code
7. Author(s) Dr. Michele V. Manuel Edward George, P.E.	8. Performing Organization Report No.
9. Performing Organization Name and Address University of Florida 152 Rhines Hall 549 Gale Lemerand Drive Gainesville, Florida 32611	10. Work Unit No. (TRAIS)
	11. Contract or Grant No. BDV31-977-02
12. Sponsoring Agency Name and Address Florida Department of Transportation 605 Suwannee Street, MS 30 Tallahassee, FL 32399	13. Type of Report and Period Covered Final Report April 24, 2013 – October 31, 2014
	14. Sponsoring Agency Code

15. Supplementary Notes

16. Abstract

High-strength low-alloy (HSLA) weathering steels are the conventional material used for non-redundant fracture-critical members in bridge construction. Guidelines have been put in place by state Departments of Transportation (DOTs) to prevent material suppliers from making scribe marks that will remain on the surface of fracture-critical members when in service, due to the possibility of degrading mechanical properties. Currently, any automated scribing marks allowed, namely mechanical milling, are either cut off of the member or subsequently welded over, thereby effectively removing them prior to service. All other markings are either manually die-stamped or spray-painted on. The lack of an automated capability to place markings on weathering steels slows production, and markings are often accidentally removed during sand blasting or shipping, which causes additional problems for the manufacturer and recipient. There is a need to establish safe, automated methods of scribing fracture-critical members such that markings will remain throughout the production process, but will not compromise the integrity over the lifetime of the part. Three automated techniques were of interest in this study as they are often already in the manufacturing process. These include mechanical milling, plasma scribing, and laser scribing. In this study, a microstructural evaluation of 50W weathering steel was conducted to understand and characterize the effect of the three markings on microstructural evolution and mechanical properties. Plasma scribing resulted in the most noticeable surface marking. S-N curves generated through fatigue testing showed no measurable difference in fatigue life between marked and unmarked material.

17. Key Word	18. Distribution Statement
Fatigue Life Notch Sensitivity Weathering Steel Automated Layout Heat-Affected Zone	No restrictions.

19. Security Classif. (of this report)	20. Security Classif. (of this page)	21. No. of Pages	22. Price
Unclassified.	Unclassified.	50	

Acknowledgements

The author's group would like to acknowledge Veritas Steel, formerly PDM, and Tampa Tank for technical discussions and for supplying and marking the weathering steel. In particular, Rick Sherman and Dale Ison are gratefully acknowledged for their efforts and discussions. Additionally, we would like to acknowledge three undergraduate students, Shrishti Shrivastava, Emma Faulkner, and Peter Feldtmann, for the hard work that they put in on the project. The undergraduate researchers were partially supported by the National Science Foundation (NSF) Research Experience for Undergraduates (REU): Infrastructure Materials program. Lastly, we thank the Major Analytical Instrumentation Center (MAIC) at the University of Florida for providing a facility where our materials characterization needs were met.

Executive Summary

High-strength low-alloy (HSLA) weathering steels are the conventional material used for non-redundant *fracture-critical members* in bridge construction. Due to the sensitivity of mechanical properties to microstructure, the American Society for Testing and Materials (ASTM) and American Association of State Highway and Transportation Officials (AASHTO) have created standards for composition, processing, and properties of weathering steels. This ensures consistent and predictable properties. Additionally, guidelines have been put into place by state Departments of Transportation (DOTs) to prevent material suppliers from making marks that will remain on the surface of fracture-critical members when in service due to the possibility of degrading mechanical properties. Currently, any automated scribing marks allowed, namely mechanical milling, are either cut from the part, or subsequently welded over, thereby effectively removing them prior to service. All other markings are either manually die-stamped or spray-painted on. The lack of an approved automated capability to place markings on weathering steels slows production, and markings are often accidentally removed during sand blasting or shipping, which causes additional problems for the manufacturer and recipient. There is a need to establish safe, automated methods of scribing fracture-critical members such that markings will remain throughout the production process, but will not compromise the integrity over the lifetime of the part. In this study, a microstructural evaluation of the bulk material and the changes which occur around the markings were investigated. Fatigue testing was conducted on marked and unmarked specimens and S-N curves were generated to elucidate the effect of the different marking techniques on fatigue life.

Four ¼”-thick plates of 50W weathering steel were scribed, sandblasted, and weathered. Tensile and fatigue specimens were fabricated through electrical discharge machining (EDM) prior to testing. The material conformed to ASTM and AASHTO standards for composition, microstructure, and tensile properties. Examination of the sample surface and microstructure around the notches revealed that the mechanical milling notch was insufficient due to lack of visibility, while the laser left a fine line that was visible but created little damage to the underlying material microstructure. The plasma scribe left the deepest mark and resulted in a heat-affected zone (HAZ). This left an effective notch of 12 mils for the plasma scribe. The fatigue life of the marked material was not measurably different from the fatigue life of the unmarked material. While plasma left the most significant mark, only two of the 16 plasma-scribed samples failed at the mark. These findings suggest that the conditions and techniques of marking used in this study are safe for implementation, but due to the limited sample size used to generate the S-N curves and the large scatter of data inherent to fatigue testing, a recommendation is made that a statistically significant study with a larger sample size be conducted to ensure safety within a greater degree of confidence. The future implementation of these automated techniques would reduce the cost and time of production for steel companies while maintaining the high standards for safety necessary for fracture-critical members of bridges.

Table of Contents

List of Figures

List of Tables

List of Acronyms

AASHTO	American Association of State Highway and Transportation Officials
ASTM	American Standards for Testing and Materials
γ	Austenite
C	Carbon
Fe_3C	Cementite
Cr	Chromium
Cu	Copper
DOT	Department of Transportation
α-Fe	Ferrite
HAZ	Heat-Affected Zone
HSLA	High-Strength Low-Alloy Steel
Fe	Iron
ksi	Kilopound per Square Inch
Mn	Manganese
MPa	MegaPascal per Square Inch
Mo	Molybdenum
Ni	Nickel
Nb	Niobium
N	Nitrogen
OES	Optical Emission Spectroscopy
OM	Optical Microscopy
O	Oxygen
α-Fe + Fe_3C	Pearlite
P	Phosphorus
Q+T	Quench and Temper
SEM	Scanning Electron Microscopy
Si	Silicon
S	Sulfur
V	Vanadium

1. Introduction

High-strength low-alloy (HSLA) weathering steels are the conventional material used for non-redundant *fracture-critical members* in bridge construction.[1-3] Due to the sensitivity of mechanical properties to microstructure, the American Society for Testing and Materials (ASTM) [3-5] and American Association of State Highway and Transportation Officials (AASHTO) [6] have created standards for composition, processing, and properties of weathering steels. This ensures consistent and predictable properties. Additionally, guidelines have been put in place by state Departments of Transportation (DOTs) to prevent material suppliers from making scribe marks that will remain on the surface of fracture-critical members when in service due to the possibility of degrading mechanical properties.[6, 7] Currently, any automated scribing marks allowed, namely mechanical milling, are either cut from the end of the part, or subsequently welded over, thereby effectively removing it prior to service. All other markings are either manually die-stamped or spray-painted on.[6, 7] The lack of an automated capability to place markings on weathering steels slows production, and markings are often accidentally removed during sand blasting or shipping, which causes additional problems for the manufacturer and recipient.[8] There is a need to establish safe, automated methods of scribing fracture-critical members such that markings will remain throughout the production process, but will not compromise the integrity over the lifetime of the part. Three automated techniques are of interest as they are already in the manufacturing process line. These include mechanical milling, plasma scribing, and laser scribing. In this study, a microstructural evaluation of the bulk material and the changes which occur around the three markings were investigated. Possible implications of these results are discussed. Fatigue testing was conducted to establish the viability of using automated marking techniques on weathering steel by comparing the fatigue life of marked and unmarked material.

2. Background

High-strength low-alloy (HSLA) steels are desirable for structural transportation applications due to their high strength to weight ratio, ductility, toughness and corrosion resistance.[1-3, 9] This study focuses on one particular grade of weathering steels referred to as 50W (or 345W), where the numbers designate the minimum yield strength requirements in ksi (or MPa). Grade 50W is considered a conventional weathering steel as it has been commonly used as fracture-critical members for bridge construction over several decades.[1, 10, 11] While the mechanical properties are generally well-established [1, 3, 10, 12], strict guidelines from state Departments of Transportation (DOTs) prevent material suppliers from making scribe marks that will remain on the surface of fracture-critical members when in service. In this study, it is hypothesized that markings may have the potential to accelerate fatigue failure. Currently, any automated scribing marks allowed, namely mechanical milling, are either cut from the end of the part, or welded over thereby effectively removing it prior to service. All other markings are either manually die-stamped or spray-painted on. The lack of an automated capability to place markings on weathering steels slow production and are often accidentally removed during sand blasting or shipping, which causes further problems for the manufacturer and recipient.[8] There is a need to establish safe automated methods of scribing fracture-critical members such that markings will remain throughout the production process, but will not compromise the integrity over the lifetime of the part. Thus, a compilation of the current state of the literature regarding microstructure and mechanical properties is presented.

2.1 HSLA Weathering Steels

High-strength low-allow steels are microalloyed with a variety of elements, including but not limited to, manganese (Mn), phosphorus (P), sulfur (S), silicon (Si), chromium (Cr), nickel (Ni), copper (Cu), niobium (Nb), and vanadium (V). Specific compositions vary depending on minimum and desirable property requirements.[3] These property requirements typically include strength, toughness, formability, and corrosion resistance. Because this class of steels is based on several minimum property requirements, grades are standardized to an extent, but many are proprietary and, thus, compositions and processing may vary from supplier to supplier. The distinction of HSLA from low carbon steels is based on the microalloying and processing techniques. Additionally, HSLA steels are not referred to as alloyed steels generally due to their low alloy content (< 3 wt%) and cost aligning with carbon steels.[9]

2.1.1 Processing and Microstructure

Steels can undergo a wide variety of processing techniques to arrive at desired microstructures and properties. The inherent link between certain microstructural features and mechanical properties allows the metallurgist to design processing routes that take advantage of nucleation, growth and shape of the resulting microstructure on several length scales. The goal for HSLA steels is to refine the ferrite (α-Fe) grain size and pearlite (alternating layers of α-Fe and Fe_3C) regions to enhance strength and impact toughness.[1] Generally, fatigue life increases with the increase in yield strength. Because the microstructure ultimately depends on processing, it is logical to discuss this first, though an introduction to the phases present throughout processing is necessary to bring relevance to the processing routes.

In order to form a uniform, fine-grained microstructure, these α-Fe and Fe_3C must be precipitated from the parent phase, γ-austenite, at elevated temperatures (this can be seen in Figure 2-1) where grain growth can become excessive.[13-15] In conventional low carbon steels, this microstructure is processed through basic solution treatments by heating the cast material to the γ-austenite region and cooling to below the eutectoid temperature of approximately 730°C. The cooling rate, soak temperature and time below the eutectoid temperature determine the scale of the microstructure, as well as the pearlite lamellar spacing.[14, 15] There is a limit to refinement through conventional means in low carbon steels that constrains the upper strength levels of this material. Through the addition of alloying elements (V, Ti and Nb), greater strength has been accomplished in HSLA steels.[9, 16, 17] Along with solid-solution and precipitation strengthening, these elements aid in refining the microstructure. In addition to this

mechanism of refinement, further refining of the γ-austenite is realized through *controlled rolling*, or Thermo-Mechanical Controlled Processing (TMCP).[14, 18] This process consists of a series of rolling steps that begin with repeated high temperature rolling (roughing) operations. Once sufficiently refined, the material is brought to a lower Austenitic temperature and hot rolled again (finishing) to flatten the γ-austenite grains (Figure 2-2).[18] After this stage, the material is cooled through the Eutectoid temperature and fine microstructure is formed. The details of the process, including hot rolling temperatures, soak temperatures and cooling rates, are not specified due to differing processing routes among steel suppliers. For Grades HPS-70W and higher yield strength, the controlled rolling process is followed by a quench and temper (Q + T) treatment in order to improve strength while remaining ductile.[12, 19-21] Efforts have been undertaken to avoid the Q + T treatment to make the processing more efficient[21, 22] and some are in service, though the details are absent from the literature likely for proprietary reasons. The main setback concerning HPS-70W TMCP steels is a lack of consistency in meeting the minimum yield strength requirements.[22, 23]

2.1.2 Microalloying in Ferrite-Pearlite Steels

The goal of microalloying in HSLA steels is to achieve higher strength and improve corrosion resistance, while conserving or exceeding the toughness and ductility of conventional low carbon steels.[1] This can be seen in the phase diagram in Figure 2-1. To increase strength, the carbon content is increased to form a larger volume fraction of cementite (Fe_3C), though this limits weldability and reduces toughness. Additions of V (<0.10%) have been shown to improve strength through solid solution strengthening as being a strong carbide former.[1, 9, 17] In grades 70W and above, nitrogen (N) is introduced and reacts with V to form vanadium nitride (VN) and carbonitride (CN) precipitates. Small amounts of aluminum (Al) also form nitrides in HSLA steels. Both carbides and nitrides assist in impeding grain growth during hot rolling and annealing [9, 15, 16], refining the microstructure. The introduction of these CN formers allows for the C-content to remain low. Additions of Cr, Ni, Cu and P can impart solid solution strengthening and enhance corrosion resistance up to four-fold over that of conventional carbon steels.[1]

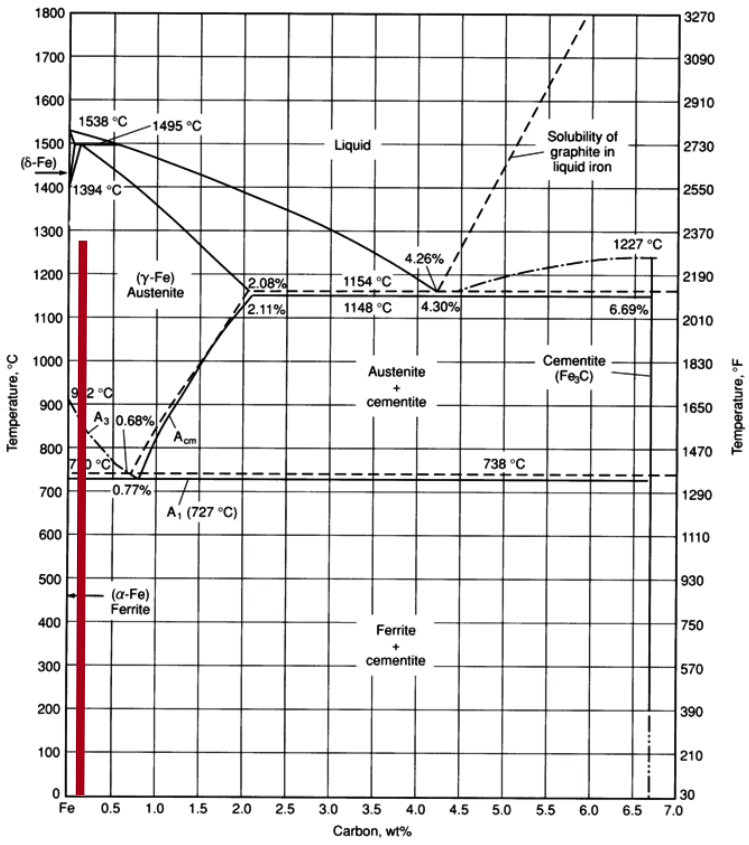

Figure 2-1: Iron (Fe) and carbon (C) phase diagram.[2] Highlighted in red is the allowable C range for ASTM A709/A709M.

2.1.3 ASTM A709/A709M and AASHTO Guidelines

The American Society for Testing and Materials (ASTM) A709/A709M: *Standard Specification for Structural Steel for Bridges [3]* outlines seven grades of weathering steels, listed in Table 2-1. Of particular interest for this review is 50W and HPS-70W. For a given grade of steel, more specified standards are outlined based on the direct

application of a member. For example, Specification A588/A588M applies to Grade 50W and outlines required compositional ranges and tensile properties, while Specification A6/A6M applies to several

Table 2-1. Seven grades of weathering steel outlined by ASTM A709/A709M.[3]	
Grade U.S. [SI]	Yield Strength, ksi [MPa]
36 [250]	36 [250]
50 [345]	50 [345]
50S [345S]	50 [345]
50W [345W]	50 [345]
HPS 50W [HPS 345W]	50 [345]
HPS 70W [HPS 485W]	70 [485]
HPS 100W [HPS 690W]	100 [690]

grades and outlines acceptable processing techniques and the resulting microstructures and mechanical properties required for the application.[4] These standards, along with the American Association of State Highway and Transportation Officials (AASHTO) Guidelines [6], must be met for each heat (or each member for fracture-critical members) in order to be put into service. Currently, there are no tests performed in industry to evaluate the fatigue properties of a particular heat because these properties are assumed to be adequate based on the required values for impact toughness and yield strength according to ASTM A709/A709M.[3] However, AASHTO *Load and Resistance Factor Design (LRFD): Bridge Design Specifications* does outline appropriate fatigue design categories for bridges (as seen in Figure 2-2). These include Categories A-E' which outline the stress range and fatigue limits required for a given member, where Category A has the highest stress range (approximately 200 MPa) and Category E' has the lowest stress range (approximately 20 MPa). The fatigue limit is reached when a specimen does not fail after 2,000,000 cycles.

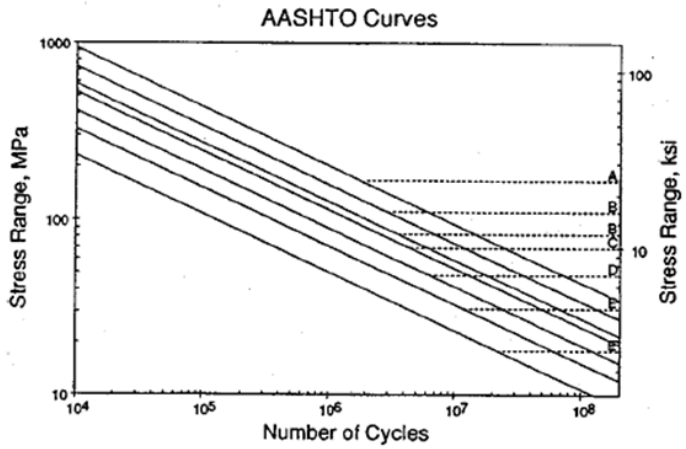

Figure 2-2. AASHTO fatigue strength categories.[6]

2.1.4 Grade 50W

Grade 50W is a fine-grained ferritic, high strength-low alloy (HSLA) steel with a low volume fraction (~0.05) of the pearlite phase (α-ferrite + Fe_3C-cementite).[1, 17] This conventional structural weathering steel is used primarily for redundant and non-redundant fracture-critical members in bridge construction.[3] It has a high specific strength and enhanced environmental corrosion resistance, compared to conventional low carbon steels [1] and is generally used in the as-rolled condition, of which,

the resulting microstructure and properties follow ASTM Standards.[3] It should be noted that this grade of steel is based on minimum property requirements, so as long as an HSLA weathering steel meets the standards of ASTM A709/A709M and ASTM A588/A588M; then they can be classified as Grade 50W (chemical compositions of 50W, according to ASTM A709/A709M, are shown in Table 2-2). This can give rise to reasonably significant variations in yield strength, ductility, and ultimately, fatigue life from supplier to supplier.

Table 2-2. Chemical composition requirements for 50W steel as described by ASTM A709A/A709M.[3]

Element	ASTM Standard for 50W
Carbon	**0.19 max**
Manganese	**0.80-1.25**
Phosphorus	**0.04 max**
Sulfur	**0.05 max**
Silicon	**0.30-0.65**
Nickel	**0.40 max**
Chromium	**0.40-0.65**
Copper	**0.25-0.40**
Vanadium	**0.02-0.10**

2.2. Mechanical Properties

The superior mechanical properties of HSLA steels over conventional low carbon steels are a result of microalloying and processing.[1] Moreover, the interplay of microstructural characteristics and mechanical properties has allowed researchers to design HSLA steels with optimized properties. The following will be a discussion of the effect of microstructure on impact toughness, yield strength, and fatigue behavior.

2.2.1 Impact Toughness

Charpy V-Notch (CVN) testing is a convention within the steel industry as a means of quality control and grade assignment.[3] In the case of *fracture-critical members*, each member must exceed the minimum standards required by AASHTO and ASTM A709/A709M for both tensile and toughness properties. For *non-fracture-critical members*, only a single randomly selected member in a heat is tested for minimum property requirements. Table 2-3 displays the required impact energy values at the given minimum use temperatures, designated as Zones 1-3. These values vary depending on required temperature range, grade, and thickness. For grades of lower yield strength which conform to ASTM A709/A709M (Grades 50, 50W, HPS-50W, etc.), the low temperature limit of Zone 3 is -12°C, and the minimum allowable impact energy at this temperature is 34 J for plate thickness of 2" and below, and 41 J for plate thickness of 4" and below. For higher yield strength grades (HPS-70W and HPS-100), the lower temperature and toughness limits are -23°C and -34°C, respectively, and 48 J for each. Generally, toughness for this class of steel far exceeds the required standards and tends to be in the range of 80-150 J at approximately -30°C. There is a wide variation in measured impact energy from supplier to supplier due to varied composition and processing routes.[1, 3] Generally, the steels which undergo a Q + T treatment have more homogenous properties from plate to plate, and across the width of each plate. Additionally, the Q + T treatments help to ensure properties which far exceed the minimum property requirements, as shown in several studies. [19-22, 24]

Table 2-3. Impact energy values for all grades of steel under ASTM A709/A709M.[3]

Grade	Thickness, in. [mm]	Minimum Test Value Energy,[A] ft-lbf [J]	Minimum Average Energy[A], ft·lbf [J]		
			Zone 1	Zone 2	Zone 3
36F [250F]	to 4 [100], incl	20 [27]	25 [34] at 70°F [21°C]	25 [34] at 40°F [4°C]	25 [34] at 10°F [−12°C]
50F [345F][B], 50SF [345SF][B], 50WF [345WF][B]	to 2 [50], incl	20 [27]	25 [34] at 70°F [21°C]	25 [34] at 40°F [4°C]	25 [34] at 10°F [−12°C]
	over 2 to 4 [50 to 100], incl	24 [33]	30 [41] at 70°F [21°C]	30 [41] at 40°F [4°C]	30 [41] at 10°F [−12°C]
HPS 50WF [HPS 345WF][B]	to 4 [100], incl	24 [33]	30 [41] at 10°F [−12°C]	30 [41] at 10°F [−12°C]	30 [41] at 10°F [−12°C]
HPS 70WF [HPS 485WF][C]	to 4 [100], incl	28 [38]	35 [48] at −10°F [−23°C]	35 [48] at −10°F [−23°C]	35 [48] at −10°F [−23°C]
HPS 100WF [HPS 690WF]	to 2½ [65], incl	28 [38]	35 [48] at −30°F [−34°C]	35 [48] at −30°F [−34°C]	35 [48] at −30°F [−34°C]
	over 2½ to 4 [65 to 100], incl	[D]	Not permitted	Not permitted	Not permitted

[A] The CVN-impact testing shall be at "P" frequency in accordance with Specification A673/A673M except for plates, for which the sampling shall be as follows:
(1) As-rolled (including control-rolled and TMCP) plates shall be sampled at each end of each plate-as-rolled.
(2) Normalized plates shall be sampled at one end of each plate, as heat treated.
(3) Quenched and tempered plates shall be sampled at each end of each plate, as heat treated.

[B] If the yield point of the structural product exceeds 65 ksi [450 MPa], the testing temperature for the minimum average energy and minimum test value energy required shall be reduced by 15°F [8°C] for each increment of 10 ksi [70 MPa] above 65 ksi [450 MPa]. The yield point is the value given in the test report.

[C] If the yield strength of the structural product exceeds 85 ksi [585 MPa], the testing temperature for the minimum average energy and minimum test value energy required shall be reduced by 15°F [8°C] for each increment of 10 ksi [70 MPa] above 85 ksi [585 MPa]. The yield strength is the value given in the test report.

[D] Not applicable.

Table 2-4 lists the mechanical properties of a variety of HSLA alloys used in bridge applications. The HPS-70W (Q + T) steel showed the highest average impact energy at 191 J, which far surpasses the minimum required energy of 48 J shown in Table 2-3.[21] These types of results are consistently observed throughout industry and in the literature. However, the newer TMCP steels have greater variation in toughness from plate to plate and across the width of a given plate.[19] Across all grades and processes, the properties tend to be consistent along the rolling direction, while varying traverse to the rolling direction, from edge to center across the width.

Table 2-4. Impact toughness at 23°C (CVN), yield strength (σ_{ys}), ultimate tensile strength (σ_{UTS}), elongation (%EL) of several weathering steels.[10, 19, 21]

		CVN (J) (@ -23°C)	σ_{YS} (MPa)	σ_{UTS} (MPa)	%EL
A588 (50W)		---	427	600	24
HPS-70W (Q+T)		---	513	613	27
		191	578.5	661.2	---
HPS-70W (TMCP)	12.7-51 mm	175	542	662	---
	22 mm	188	490.2	653.6	26.3
	51 mm	115	415.1	661.2	30.7

It is important to note the variation in properties as a function of plate thickness. The average CVN energies for some HPS-70W TMCP steels are shown in the bottom three columns of Table 2-4. Most notably, one study showed an average CVN energy of 175 J over a range of thicknesses (0.5-2”), but did not report a variation [21], while another showed a great disparity between the thicknesses of 7/8” (188 J) and 2” (115 J).[19] A schematic from this study of impact energy across the plate is shown in Figure 2-3.

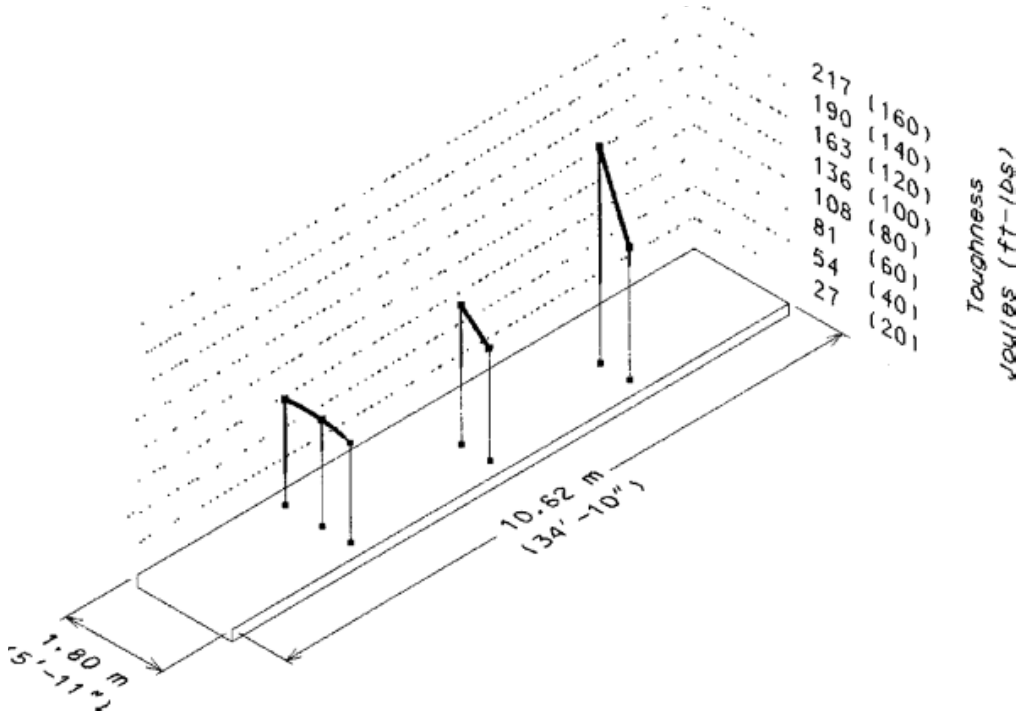

Figure 2-3. Impact energy with respect to position on a plate of HPS-70W TMCP.[19]

Plate thickness was found to have a great effect on the resulting properties due to cooling rates during hot rolling procedures. Coarsening and phase transformations resulted in limited impact energy for the thicker plate.[19] Alloying elements that form carbonitrides can contribute to this effect, as well. In some V and

V + Nb HSLA steels, longer aging times have resulted in lower measured CVN energy values and higher ductile-to-brittle transition temperatures (DBTTs) due to the increased formation and growth of these small, brittle particles. Limiting the aging time and temperature proved to preserve toughness in the V and Nb + V HSLA steels.[23] Regardless of the wide range of impact energy values across the width and over varying plate thicknesses, each group of specimens from all studies reviewed exceeded the minimum required values and the variation was not considered an issue for application.

2.2.2 Yield Strength

Just as CVN testing is a measure of toughness and ductility of steel, tensile testing is used as a measure of strength, for both fracture-critical members and non-fracture-critical members. The material must conform to the minimum yield strength requirements outlined by the standard ASTM A709/A709M. The yield strength varies in these steels due to the allowable range of composition and processing for a given grade. On a microstructural level, the yield strength generally depends on the refinement of the γ-austenite grains at elevated rolling temperatures, the refinement during finishing steps and the cooling rates[1], though, control of the cooling rate is limited by the thickness of the plate. This is the main reason why properties depend on plate thickness, and, thus, why standardizing plate thickness is emphasized in ASTM A709/A709M. Additionally, the Q + T treatment results in enhanced strength and toughness by the precipitation of carbonitrides and the dissolution of martensite (a metastable phase which forms during rapid cooling from elevated temperatures). Though properties have been shown to vary from heat to heat, the employment of the Q + T treatment ensures that the minimum property requirements are met, regardless.

In an effort to avoid this final step (Q + T) for efficiency in processing and to produce larger members, a study at Arcelor Mittal USA Research Center [21] showed that the finishing rolling temperature had a significant effect on the as-rolled yield strength. As-rolled results from the study are shown in Table 2-5. The as-rolled yield strength nearly doubled (from 322.7 MPa to 624 MPa at 950°C and 700°C, respectively) as a result of lowering the finishing rolling temperature. The resulting CVN values were satisfactory when considering the standard requirements[3], however, the absorbed energy decreased significantly as the finishing temperature increased. The reported inconsistent strength (yield and tensile) across the width of plates of HPS-70W TMCP is displayed in the schematic in Figure 2-4.[19] The strength tends to decrease when moving from the edge of the plate to the center. HPS-70W Q + T steels were not reported to have exhibited this behavior. In this particular study, the TMCP steels rolled at 700°C adhere to the standard for both strength and toughness despite the variations within a given member, though several other studies have shown low and inconsistent yielding behavior in HPS-70W TMCP steels.[19, 20, 22, 25] Currently, most TMCP steels are not recommended for fracture-critical members of higher yield strength requirements (>485 MPa), though they are used in bridge members that conform to the property requirements of HPS-50W and 50W steels.[22] The improvement from 50W TMCP to HPS-50W TMCP lies in the enhanced weldability and lower DBTT. There is a limited body of literature evaluating the strength of conventional 50W TMCP steels as the strength was sufficient assuming appropriate quality control.[1, 3]

Table 2-5. Mechanical properties of an HPS-70W TMCP steel.[21]

	Rolling Temperature (°C)	σ_{YS} (MPa)	σ_{UTS} (MPa)	%EL	CVN (J) (@ -30°C)
As-Rolled HPS-70W	700	624	658.4	20	134
	870	414.4	603.3	21	54
	950	322.7	540.5	30	---

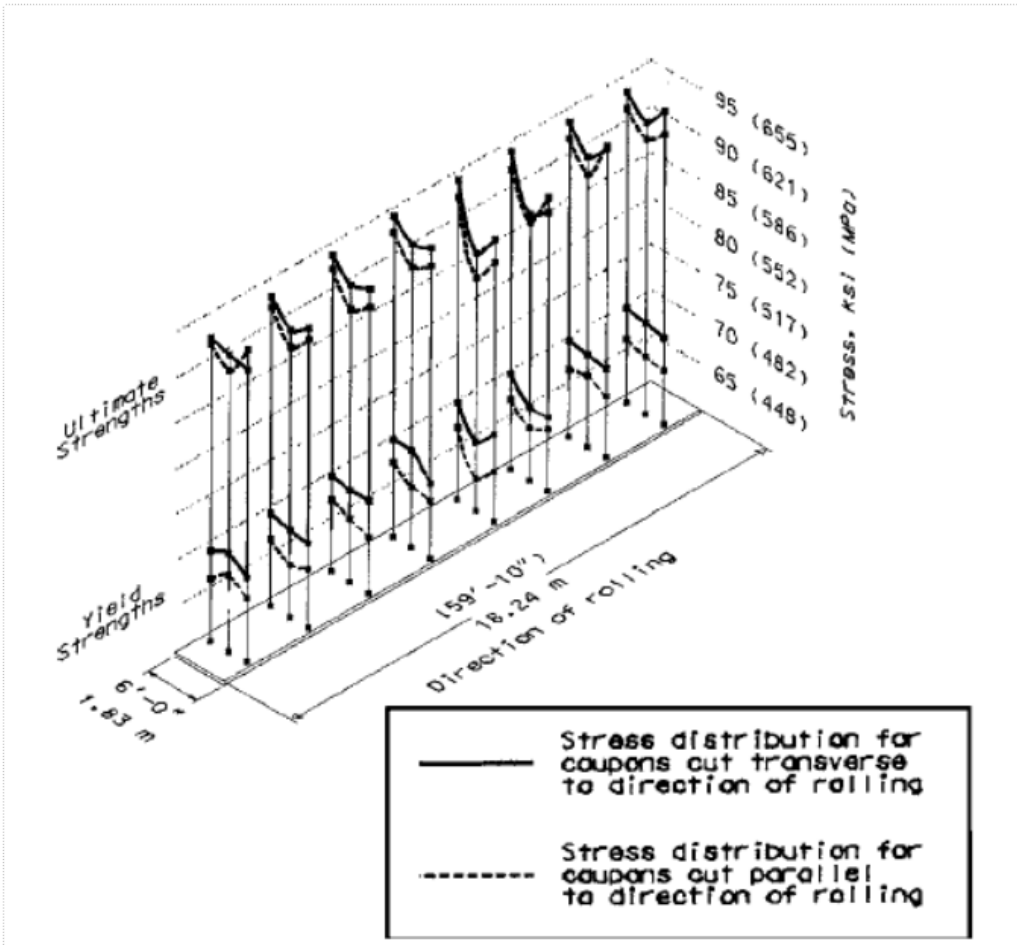

Figure 2-4. Strength with respect to position on a plate of HPS-70W TMCP.[19]

2.2.3 Fatigue of Weathering Steels

Conventional weathering steels, such as those which fall under Grade 50W, have been used for decades for bridge construction and, thus, processing routes and the resulting mechanical properties have been well established to adhere to requisite standards.[1, 3] Little current research has been published on the fatigue properties of this particular grade, with the exception of comparison with HPS properties, and of corroded members for the purpose of evaluating the environmental effects that could be affecting the lifetime of the current bridges in use. Grade 50W falls under AASHTO Category A (See Section 2.3) when the test specimen are cut directly from a rolled beam, while welded beams and cover plates are Category B. As a result of weathering rolled beams for 62 and 67 months in moist fresh water and salt water environments, respectively, the fatigue strength dropped to Categories B and E.[26] The 'sheltered' salt water environment (simulating material under a bridge) resulted in a detrimental loss in fatigue strength, while 'bold' fresh water exposure (simulating material on the side or top-side of a bridge) only called for a slight adjustment in the categorization of members under such conditions. Welded beams[10] were shown to retain much of their fatigue strength in a bold fresh water environment after 45 months, remaining in Category B. Cover plates, under the same condition for 74 months, had a loss in fatigue strength down to Category D. The fatigue strength of all welded and cover plated beams, in the sheltered salt water environment, reduced to Category E. The precise environment of a member, a weld and a cover plate must be identified in order to appropriately design a bridge to the outlined standards. Painting severely corroded bridges made of conventional weathering steel was the recommendation of this particular study.

The efforts in the early 1990's to move from conventional weathering steels resulted in a considerable amount of research into the possible advantages of the new high performance steels being developed. With microalloying and advanced processing, higher yield strength, weldability and greater toughness, at even lower temperatures, were realized. These properties would generally increase the fatigue strength as a result of the enhanced yield point.[27, 28] Results showed that polished fatigue specimens have fatigue limits in the stress ranges of 265-321 MPa, well above the requirements for Category A, which is approximately 165 MPa.[20] The fatigue behavior depends strongly on surface roughness and after applying a correction factor of 0.67 [29], a likely more realistic stress range of 200 MPa was calculated, still well above the requirements of the standard for Category A. While the fatigue limit for smooth specimens of HPS-70W proved to be superior to conventional weathering steels, some experimental evidence suggests that connection details such as welds and riveted sections of both grades have similar fatigue limits.[22]

Although literature on surface effects on fatigue performance is limited, some notch sensitivity can be inferred by studying the fatigue properties of bridge steels containing holes or rivets. Bridge connection details require welds and holes to be drilled or punched for rivets and bolts. Initially, HPS had an assumed rating for these members identical to conventional connection details due to the lack of experimental evidence allowing for a reformation of the design criteria.[6] Fatigue testing on HPS-70W and A36 (a conventional weathering steel), with circular drilled holes were evaluated for comparison.[20] Figure 2-5 shows the data gathered, along with S-N curves predicted via an inelastic finite element analysis and AASHTO Categories B and C. The slopes of the predicted curves agree well with the measured data, but vary significantly from the slope of the standard S-N curve for Categories B and C. Both steels performed better than the predicted values (labeled Design curve in Figure 2-5) and HPS-70W was well above Category B despite the lesser slope, while the conventional weathering steel fit different categories dependent on the stress range. HPS 70W with drilled holes was approximately one category greater than the conventional steel with the same sample geometry. Another study, evaluating the effects of punched, punched and reamed, and drilled holes revealed that HPS 70W adheres to the standard, Category B, for punched and reamed and drilled holes.[27] The samples with holes that were punched, but not reamed, resulted in lower fatigue life ranging between Categories C and D. Plate thickness plays a major role in the effect of punched holes.[27, 30] For thinner plates, the deleterious effect diminishes, so standards are set limiting punched holes to the thinner members.

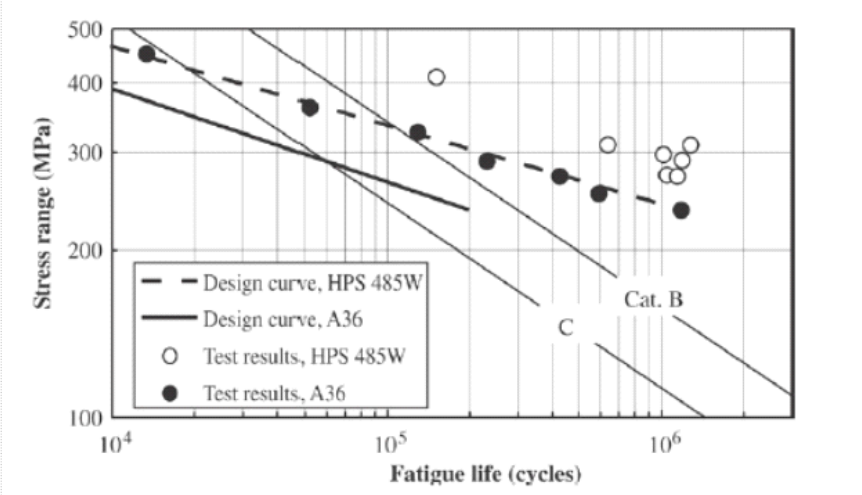

Figure 2-5. Fatigue life data from conventional (labeled A36) and HPS 70W (labeled HPS 485W) weathering steels with drilled holes represented as solid and open circles, respectively.[20]

There is an absence of evidence in the literature defining the effects of surface flaws on the outer surfaces of fracture-critical members of both HPS and conventional weathering steels. The current undertaking by FDOT and the University of Florida aims to evaluate the effect on fatigue properties of markings etched into the surfaces of fracture-critical members of bridge steels. To elucidate this effect, the notch sensitivity factor, q, can be calculated using experimental data and fracture mechanics [31] and is defined as:

$$q = (K_f\text{-}1)/(K_t\text{-}1) \qquad \text{Equation 1}$$

where K_f is related to the ratio of notch fatigue strength and smooth specimen fatigue strength, and K_t is the theoretical concentration factor for the notch. In the literature, an evaluation of notch sensitivity has been conducted comparing conventional low carbon steels with HSLA steels.[32] The study showed that the notch sensitivity for the HSLA steel was in fact slightly greater than that of the low carbon steel. Despite this finding, the notch fatigue strength of the HSLA steel was greater due to the overall superior fatigue strength. While the overall fatigue strength is greater for HSLA steel, the notch sensitivity may have implications for the current study on the effect of surface markings on the particular class of HSLA steel outlined by ASTM A709/A709M.

2.3 Marking Technologies

Currently, the bridge steel industry relies on die stamping and other manual means of marking parts for the subsequent stages of production, or for informing the customer of heat number, grade, orientation, and weld positions.[7] These methods slow production for a variety of reasons, including marking speed, misinterpreted markings, or the loss of the marking all together via subsequent sand blasting steps. Automating this process is expected to limit the bottleneck in the production line and eliminate human error. Three automated scribing techniques have been targeted as viable options for the industry. These include mechanical milling, plasma marking, and laser marking.[8] The characterization of the markings and the underlying microstructure resulting from the marking techniques were the focuses of the current study.

2.3.1 Mechanical Milling

Mechanical mill scribing employs a conical drill bit with a rounded tip that scratches the surface, removing material at rates up to 160 inches per minute. There are several benefits to this technique. These include fewer consumables, less power consumption, and multiple surface scribing, where scribing can be conducted on up to four sides of the part.[33] An air compressor powers the scribe where gas tank storage or continuous electrical arcing is necessary. The drawbacks to this technique include a slower relative scribing speed, high capital costs, and the need to switch bits for other milling operations on the same part. Many companies already employ milling, so the initial costs can be somewhat negligible, though the need to change from bit to bit slows the milling process. Regardless, automated mechanical milling is already being used in much of the industry.[8]

2.3.2 Plasma Marking

Plasma marking, using superheated ionized gas, can be conducted with a stand-alone machine used only for marking, or in the case of the Voortman V808 [34], the same machine used for plasma cutting can be used for surface marking by adjusting the machine down to 5-15 amps. The use of the same bit for cutting and marking places it at an advantage over mechanical milling. Additionally, marking speeds up to 400 inches per minute are realized, though it is necessary to stop and restart the arc for abrupt changes in direction, thus reducing the marking speed. There are two consumable gases used for plasma, the cutting gas, hydrogen or oxygen, and the inert shielding gas, typically argon. These gases are an added cost and are used up more rapidly the more the arc stops and restarts. The high-powered arc also uses a great deal of electricity, adding to the production costs.[8]

2.3.3 Laser Marking

Laser marking is a newer scribing technique and is less ubiquitous in the industry. Writing speeds between 200 and 400 inches per minute can be achieved and the laser can continuously mark even for more complex patterns. This technique requires relative high energy usage, but the speed and lack of consumables can make up for this added cost. Additionally, lasers can scribe on up to 12 surfaces at a time.[35] Currently, its use is limited to the formation of 'dark oxidation' which is easily removed during sand blasting. In order to remove more material to form a sustainable mark, higher energy outputs would be necessary and marking time will increase. While laser has some benefits, employment of this technique would require the manufacturer to buy an additional piece of equipment, whereas with milling and plasma, the machines may already be on hand.[8]

There are challenges and benefits for each of the three techniques being considered. For the purposes of etching bridge steels, the optimal option may depend of the effect each technique on the resultant properties of the steel. Mechanical milling will introduce plastic deformation around the mark, while plasma could result in a significant heat-affected zone. Laser would be expected to have less of a heat-affected zone compared to plasma [8], but the increased depth for sustained scribing has not been evaluated. The repercussions of the damage described here can effectively increase the notch size, or initial crack size, thus, reducing the fatigue life.[36-40] Additional research is required to evaluate the possible effects.

3. Material Acquisition and Marking

Weathering steel plates of Grade 50W, rolled to ¼ inch thickness, were selected for characterization and testing based on the capabilities of the Mechanical Testing System (MTS) which were later used for fatigue testing. Veritas Steel, formerly PDM Bridge Plant, supplied 4 2.5' x 1.5' as-rolled 50W steel plates. This material has lower fatigue properties compared to other grades used for fracture-critical members [41, 42], thus, this grade represents a material with properties closest to the minimums required for the ASTM Standards and AASHTO requirements.[3, 6] The plates were sent to Tampa Tank for marking, sandblasting and weathering. Three of the plates were marked with mechanical, plasma and laser scribes, as shown schematically in Figure 3-1, such that 3 lines per scribe were oriented traverse to the rolling direction and a mechanical and laser line were placed parallel to the rolling direction. The remaining plate (#4) was left unmarked. The parameters used for scribing are shown in Table 3-1. Sandblasting was followed by weathering to achieve a smooth plate surface for even oxide formation. Weathering was conducted by showering the sandblasted plates with water.

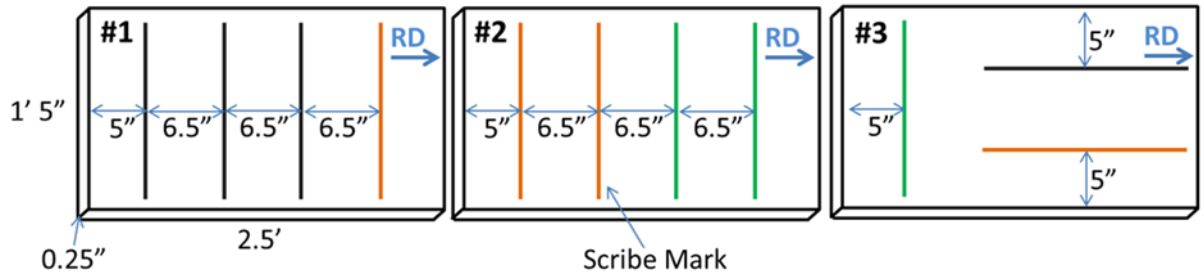

Figure 3-1. Schematic of 50W grade steel plates with mechanical milling (black), plasma (orange) and laser (green) scribed lines.

Table 3-1. Parameters of scribing techniques.

Technique	Write Speed (inch/min)	Pressure/Power/Current
Mechanical Milling	**140**	**80 psi**
Laser Scribe	**120**	**60 Watts**
HD Plasma	**250**	**10 Amps**

A photograph of Plate #1 is shown in Figure 3-2 after plasma and mechanical scribing, sandblasting and weathering. The plasma scribe resulted in a consistent, visible line, while the mechanical scribe left an inconsistent line that was not visible across much of the plate. Plate #2, in Figure 3-3, was photographed revealing consistent laser and plasma scribed lines. It should be noted that the mechanically scribed lines were inconsistent and not visible on much of the plate despite the relatively slow milling speed, as referenced in Table 3-1.

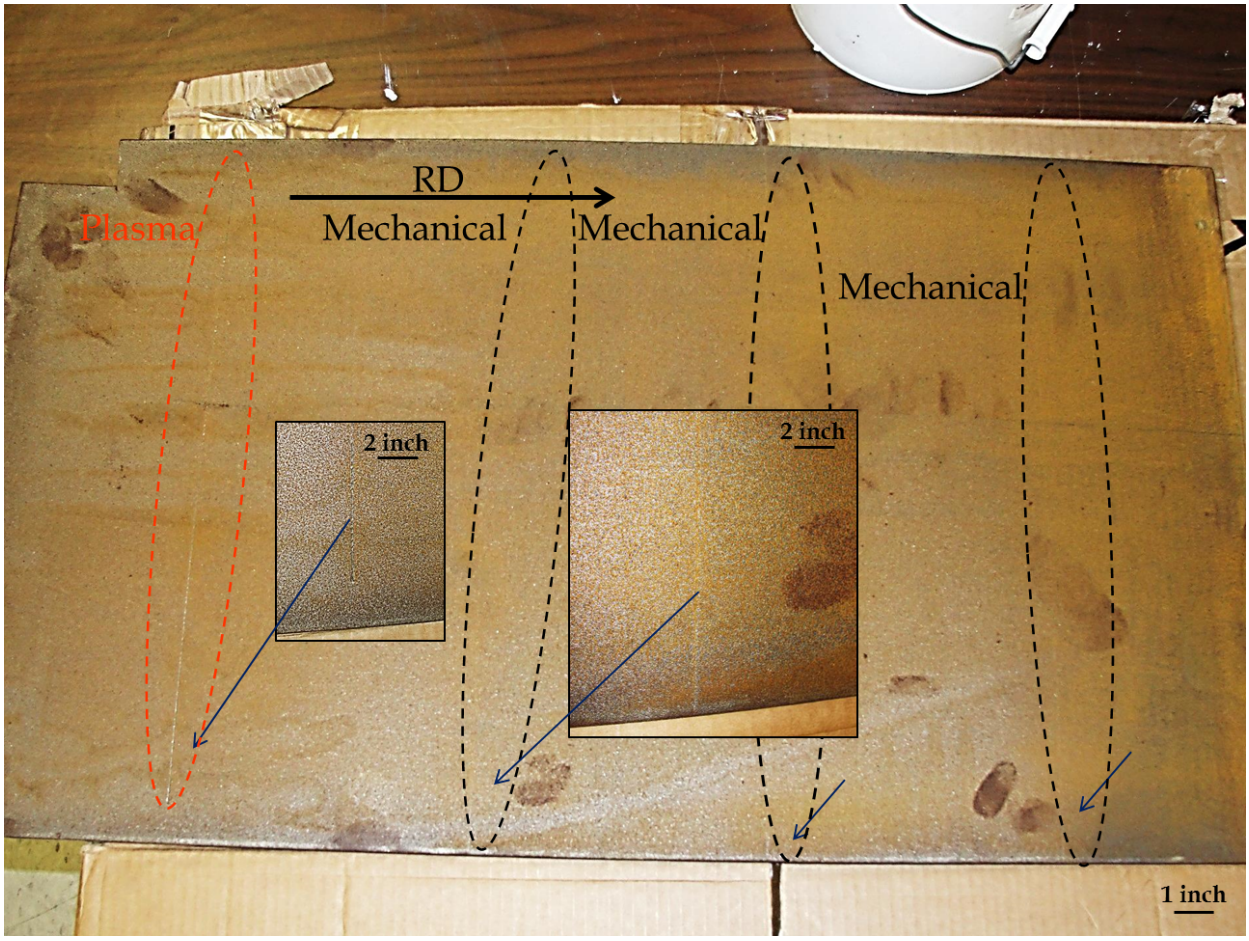

Figure 3-2. Photograph of Plate #1 showing a plasma scribe mark and three mechanical scribe marks.

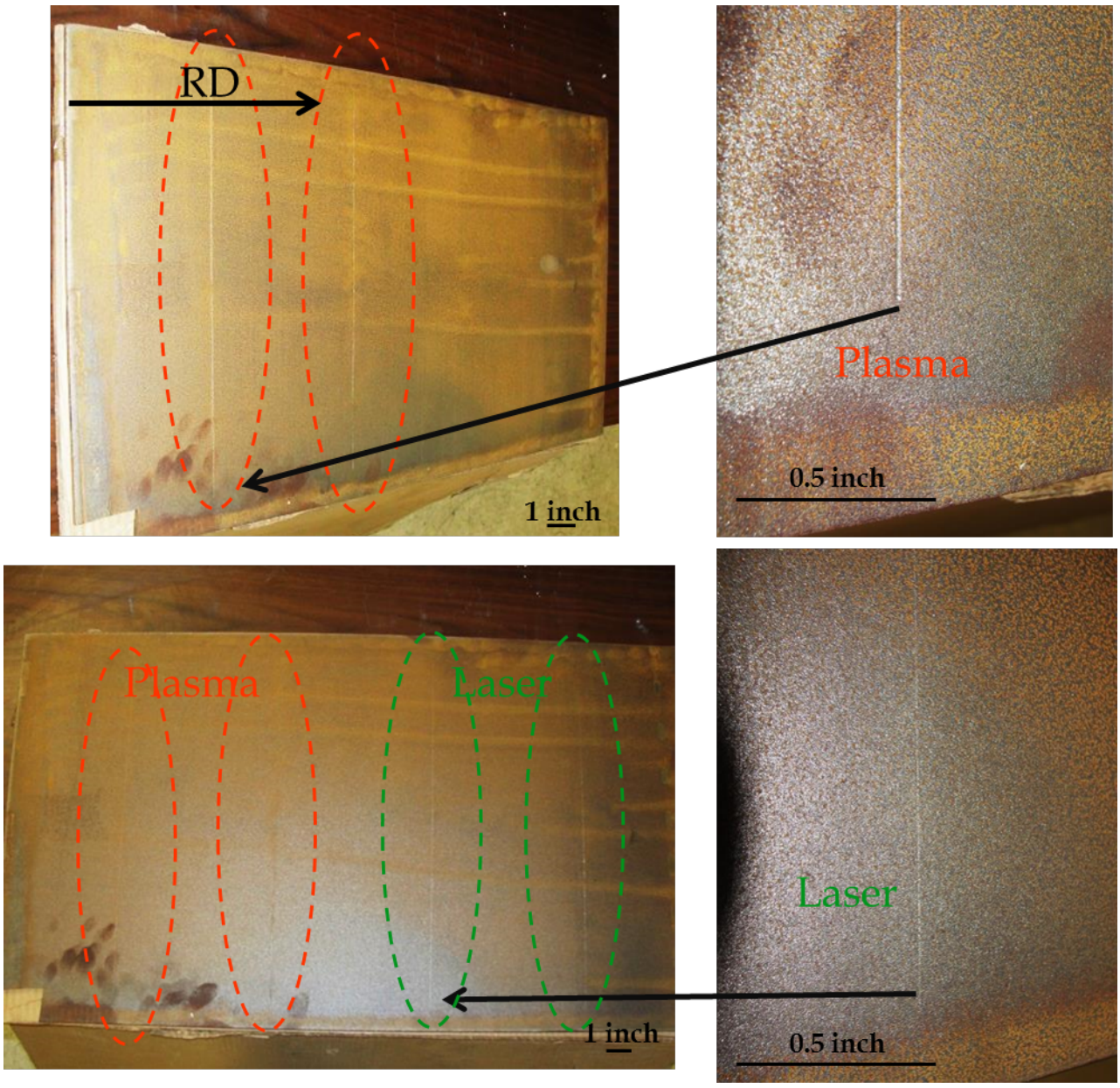

Figure 3-3. Photograph of Plate #2 showing two plasma scribe mark and two laser scribe marks.

4. Microstructural Analysis

4.1 Compositional Analysis and Sample Preparation

A coupon was taken from each plate for compositional analysis using Optical Emission Spectroscopy (OES) (See Table 4-1). The resulting compositions for the 4 plates fall in the acceptable ranges set out for a 50W grade steel. The presence of Mo can reduce DBTT and is a common trace element in HPS weathering steels.[3]

Table 4-1. Optical Emission Spectroscopy of 50W steel plates.

Element (%)	Plate #1	Plate #2	Plate #3	Plate #4	50W Nominal
Carbon	**0.07**	**0.07**	**0.06**	**0.07**	**0.16 max**
Manganese	**0.82**	**0.82**	**0.83**	**0.83**	**0.80-1.25**
Phosphorus	**0.013**	**0.013**	**0.014**	**0.015**	**0.030 max**
Sulfur	**0.006**	**0.006**	**0.006**	**0.006**	**0.030 max**
Silicon	**0.35**	**0.35**	**0.36**	**0.36**	**0.30-0.50**
Copper	**0.28**	**0.29**	**0.30**	**0.29**	**0.25-0.40**
Nickel	**0.22**	**0.22**	**0.23**	**0.23**	**0.40 max**
Chromium	**0.46**	**0.46**	**0.46**	**0.47**	**0.40-0.65**
Molybdenum	**0.02**	**0.02**	**0.02**	**0.02**	**...**
Iron	**Remainder**	**Remainder**	**Remainder**	**Remainder**	**Remainder**

Samples for microstructural evaluation were cut from the plates using a LECO MSX205M cut-off saw with abrasive aluminum oxide blades. Samples used to characterize the bulk microstructure were cut from the three orientations shown in Figure 4-1. Samples were mounted in EpoMat Molding Compound F using a LECO PR-10 mounting press at a pressure of 4200 psi and the mount was heated for 1 minute at a preset temperature. Polishing was done using 320, 600, and 800 grit SiC paper and diamond suspensions of 0.118 and 0.004 mils (3 and 0.1 μm) on polishing pads. A 3-second Nital etch (3% nitric acid & ethanol) was used to reveal microstructural features for microscopy. Samples for notch characterization were mounted with aluminum (Al) markers in order to help locate the notch.

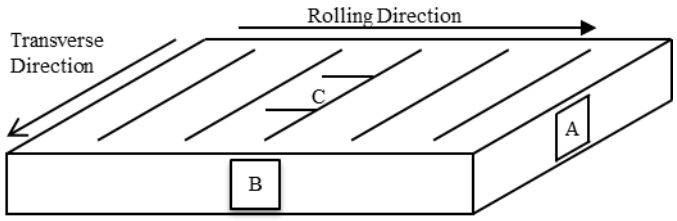

Figure 4-1. Schematic of 50W grade steel plate orientations (A) perpendicular and (B) parallel to the rolling direction and (C) on the plate surface.

Samples were imaged with a Leica DM2500M optical microscope with a ProgRes C5 camera at 50, 100, 200, and 500x magnifications. For SEM imaging an FEI XL-40 field emission SEM was used in both the secondary (SE) and backscatter (BSE) conditions. Grain size measurements, following the General Intercept Procedures in ASTM E112 – 13 [43], were conducted on optical images by drawing 10 lines of known length across the image. This was done on three images for each orientation and a representative image is shown in Figure 4-2. Grain boundary intersections were counted and Equation 1 was used to determine the grain size.

$$Grain\ Size = \frac{Length\ of\ Line}{Number\ of\ Grain\ Boundaries}$$ | Equation 2

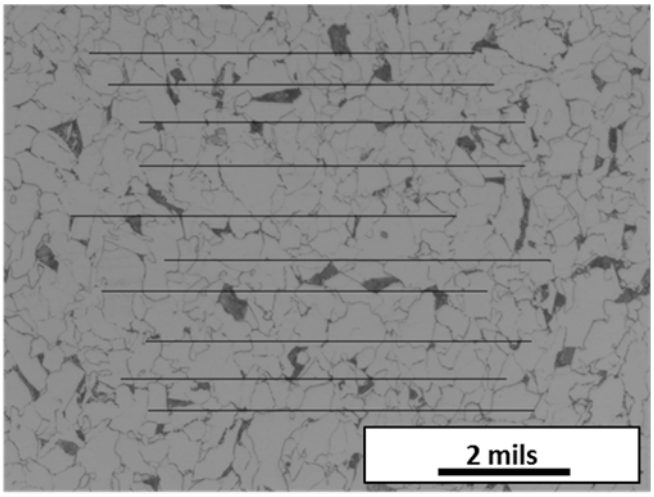

Figure 4-2. Representative optical micrograph with lines overlaid for grain size measurements following ASTM E112-13.[43]

The plasma notched sample was indented using a Buehler Mircromet II microhardness tester with a Vickers diamond indenter. Indents were placed in the bulk microstructure at 0.11, 0.44 and 2.2 lbs (50, 200 and 1000 gf), and at 10 indents per load. 10 to 15 indents, at 0.11 lbs (50 gf), were placed in each of several regions of the HAZ around the notch.

The stress concentration factor (K_t) due to the plasma notch was estimated by measuring notch width, depth, radii of curvature and sample thickness. These values were applied to charts that were experimentally determined through photoelastic stress analyses [44] to find the K_t of a material with various notch geometries. The stress concentration factor is a ratio (Equation 2) of the maximum stress at the notch (σ_{max}) and the applied far field stress (σ_{app}).

$$K_t = \sigma_{max}/\sigma_{app}$$ | Equation 3

4.2 Characterization of bulk microstructure

Metallographic samples were taken from each of the three plate orientations (A, B and C) outlined in Figure 4-3. Through optical and scanning electron microscopy, the microstructure was revealed to be fine grained α-ferrite + pearlite (eutectic α+Fe_3C). Quantitative microscopy, using the lineal intercept method [43], was conducted on each of the three orientations resulting in grain sizes of 0.319, 0.303 and 0.311 mils (8.1, 7.7 and 7.9 μm) for orientations A, B and C, respectively. These grain sizes fall in the range of ASTM grain sizes #10 and #11, which is well below the fine grain requirement of #5, outlined by ASTM A6/A6M-11.[3, 43] The material had an equiaxed morphology in all orientations, thus the plate is expected to display isotropic properties and thus behavior is not expected to be highly determinate on the relative orientation of the scribe lines. For microstructures of rolled materials, a laminated structure is typically

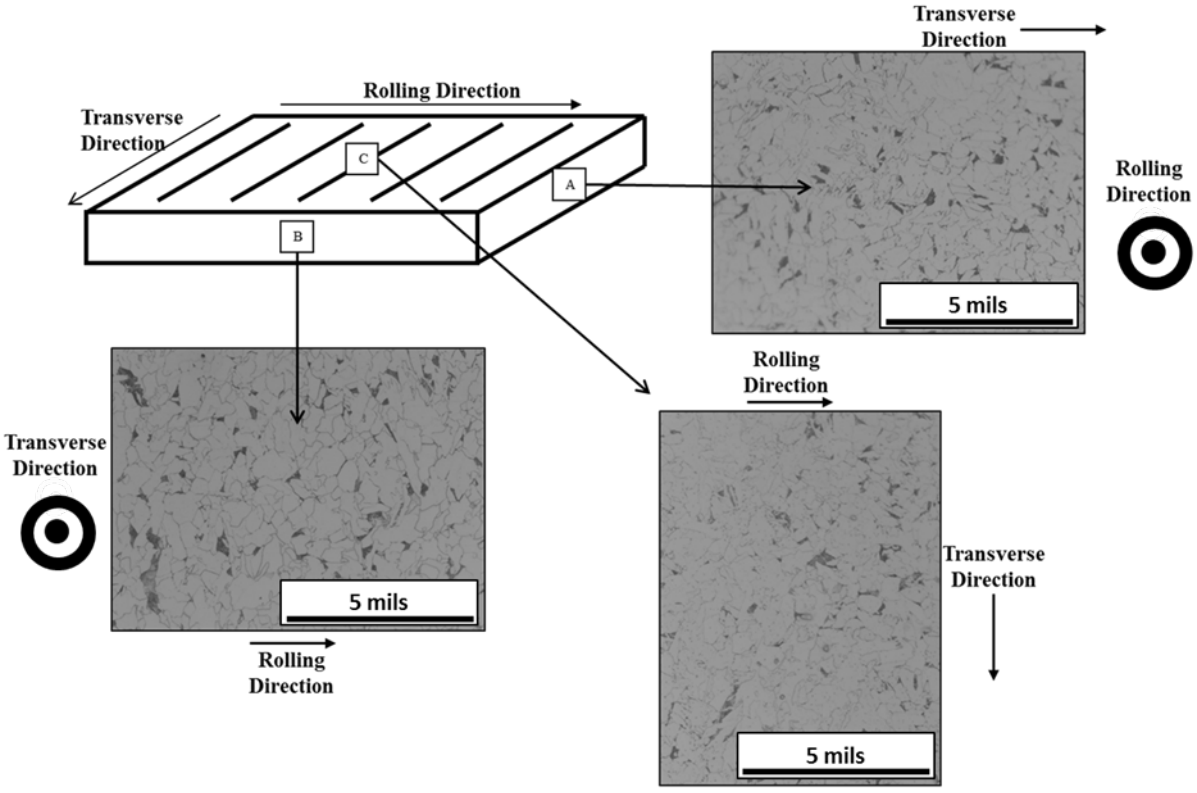

Figure 4-3. Micrographs showing equiaxed ferrite grains from each of the three plate directions.

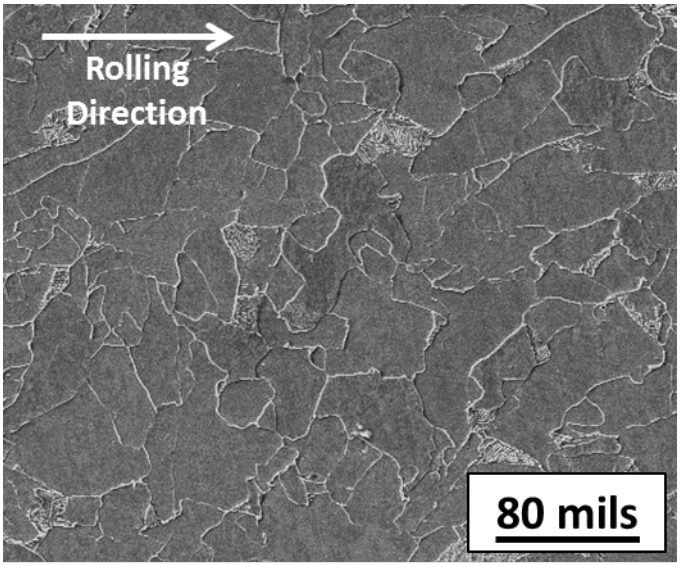

Figure 4-4. Secondary electron micrograph of 50W grade steel with equiaxed a-grain structure.

expected along with grains elongated along the rolling direction.[2] In this particular case, the material was hot-rolled with a significant reduction in thickness to ¼ inch. The strain and heat which were introduced resulted in the onset of recrystallization and, thus, the highly strained elongated structure transformed to the apparent equiaxed structure shown in the secondary electron micrographs in Figure 4-4, where the darker grains are α-ferrite and the lighter regions of lesser area fraction are pearlite. Vickers Microhardness Indentation was conducted on the bulk material on a cross section from orientation B from Figure 4-4. The load levels of 0.11, 0.44 and 2.2 lbs (50, 200 and 1000 gf), results of which are plotted in Figure 4-5, yield similar average hardness values of 197, 189 and 192 VHN or 280, 274 and 278.5 ksi (1.93, 1.85 and 1.88 GPa), respectively. The plot, in Figure 4-5, reveals a larger range of scatter for the 0.11 lbs (50 gf) indents and this is likely do to the amount of material being tested at this relatively low force. When the indent diagonals approach the grain size of a material, the orientation of the few grains sampled per indent have a significant effect on the hardness value. Essentially, with the indent diagonals on the order of approximately 0.79 mils (20 μm), the results approach single crystal behavior, which is more anisotropic. For the purposes of this study, it was important to have indent diagonals small enough such that small regions the heat-affected zone (HAZ) around the notches could be analyzed.

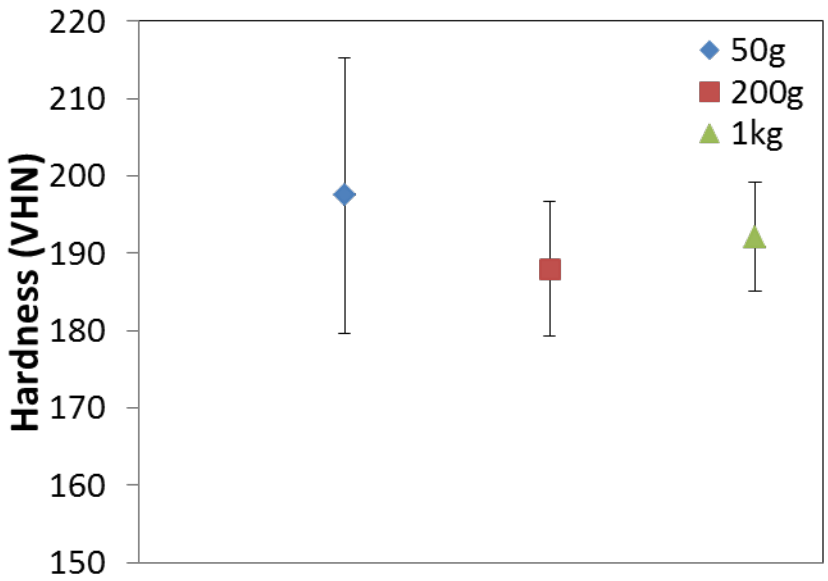

Figure 4-5. Bulk Vickers hardness values over several loads.

4.3 Characterization of Mechanical, Laser and Plasma Scribed Notches

Samples were cut from orientation B for notch characterization. The mechanical, laser and notch profiles are shown in Figure 4-6 for comparison. The mechanical milling notch profile, in Figure 4-7, shows a small notch and a limited plastic affected zone that is approximately 1.61 mils (41 μm). The affected zone has elongated grains which formed to due to the shear introduced by the milling. The profile of the laser notch is shown below the Al marker in the optical micrograph in Figure 4-8. There is a small heat-affected zone (HAZ) of approximately 0.71 mils (18 μm) located at the mark. The plasma notch, shown in Figure 4-9, has an approximate depth of 5.9 mils (150 μm) and a clearly defined HAZ on the order of 7.87 mils (200 μm). The optical micrograph in Figure 4-10 shows an enlarged view of the HAZ of the plasma notch. Several distinct morphological regions are outlined in the microstructure, which are labeled melted scale, inner, outer, border and bulk. Vickers microhardness indentation was performed on these regions and Figure 4-11 is an optical micrograph with color-coded diamonds overlaid to scale on the indents. The

thinnest region, labeled inner, was on the order of 1.18 mils (30 μm), so the lowest load level, 0.11 lbs (50 gf), was necessary to keep the dimensions of the indent within the region and this load level was used throughout this experiment for consistency in hardness values from region to region. Figure 4-12 is a plot of Vickers Hardness Number (VHN) versus the average distance from the notch surface. The hardness of the material increases 3-fold from 193 VHN, in the bulk microstructure, to 545 VHN on the plasma notch surface.

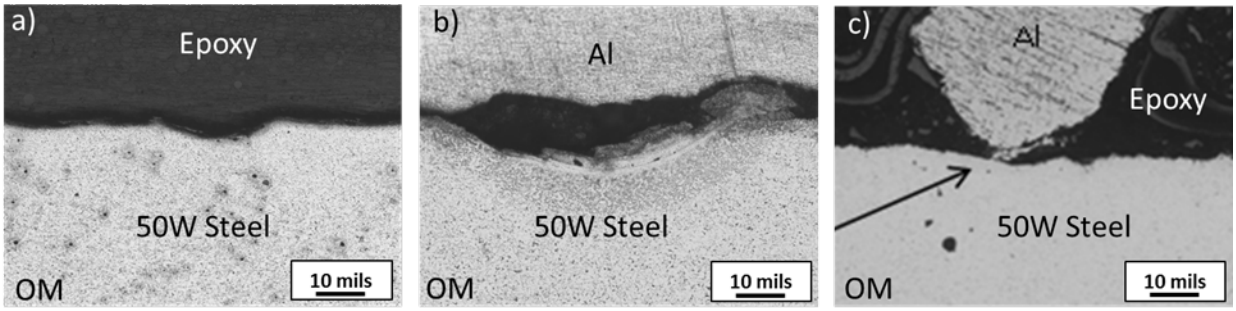

Figure 4-6. Notch profiles of a) mechanical, b) plasma, and c) laser scribed notches.

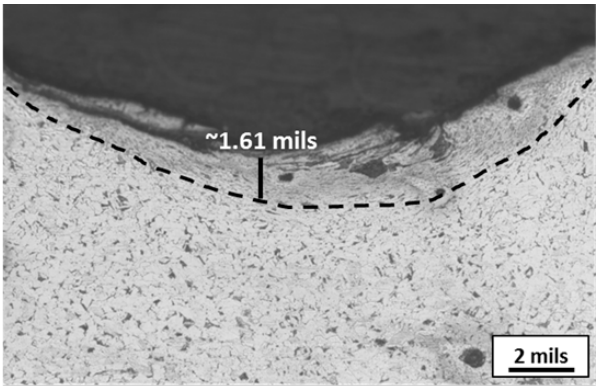

Figure 4-7. Profile of mechanically milled scribe mark with the dashed line outlining the plastic-affected zone.

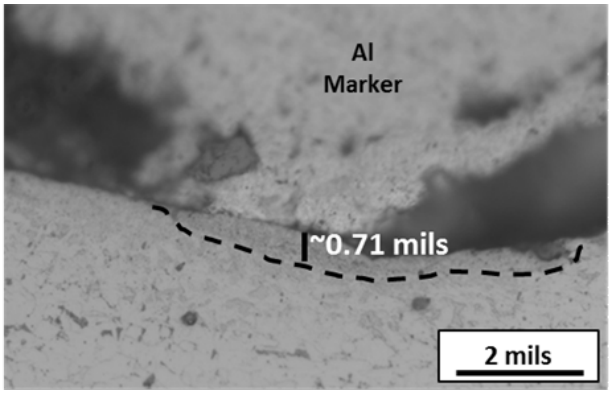

Figure 4-8. Profile of laser scribed mark with the dashed line outlining the heat-affected zone.

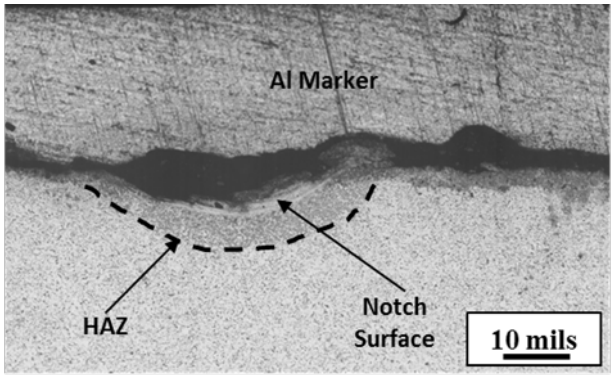

Figure 4-9. Profile of plasma scribed mark with the dashed line outlining the heat-affected zone.

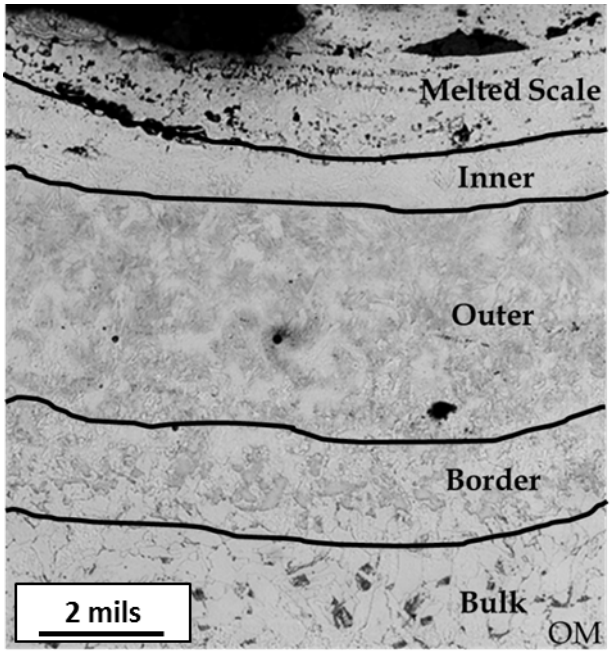

Figure 4-10. Enlarged micrograph of the HAZ caused by the plasma mark.

The notch geometry plays an important role in imparting stress concentrations, which result in higher localized stresses in the notched region. The sites with stress concentrations can result in fracture initiation at relatively low far field stresses. Photoelastic stress distributions for a variety of notch geometries were studied [44] and tables were developed that relate notch dimension ratios with stress concentration. The stress concentration factor, K_t, for the plasma notch was estimated using the notch dimensions and sample thickness. The width, 2a, depth, d, and notch radius of curvature, r, of the notch

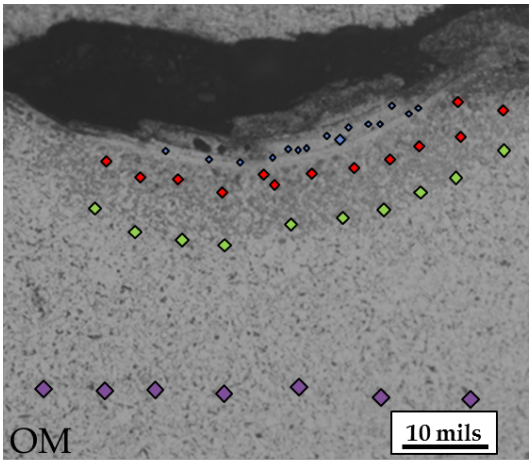

Figure 4-11. Optical micrograph of the plasma notch profile with color coded indent marks made to scale.

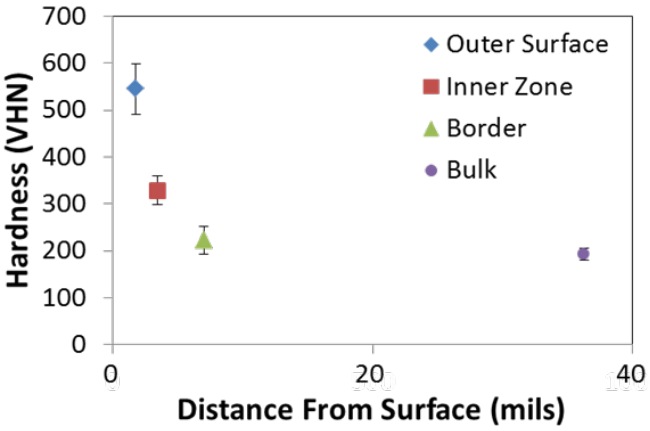

Figure 4-12. Vickers Hardness Number versus the sample depth from the plasma notch surface.

are shown in Figure 4-13. The resulting K_t of 1.7 suggests that the maximum stress reached in the vicinity of the notch is approximately 1.7 times that of the applied far field stress on the bulk of the material. When comparing the results of the hardness testing, which showed a 3-fold increase in hardness/strength at the notch surface, with the estimated stress concentration of 1.7 at the notch, it may be inferred that these effects essentially counteract each other with respect to expected effect on the mechanical properties. This is to say that the increased hardness/strength at the notch surface aids in mitigating fatigue processes despite the localized stress in this region due to the inherent stress concentration due to the notch.[45, 46] While these results are promising, other factors associated with the plasma notch may be affecting the fatigue properties, such as, refinement of the microstructure and embrittlement due to oxide formation/incorporation, each of which would be deleterious for fatigue properties. Therefore, fatigue testing is necessary in order to safely implement these scribing techniques in the processing of weathering steels.

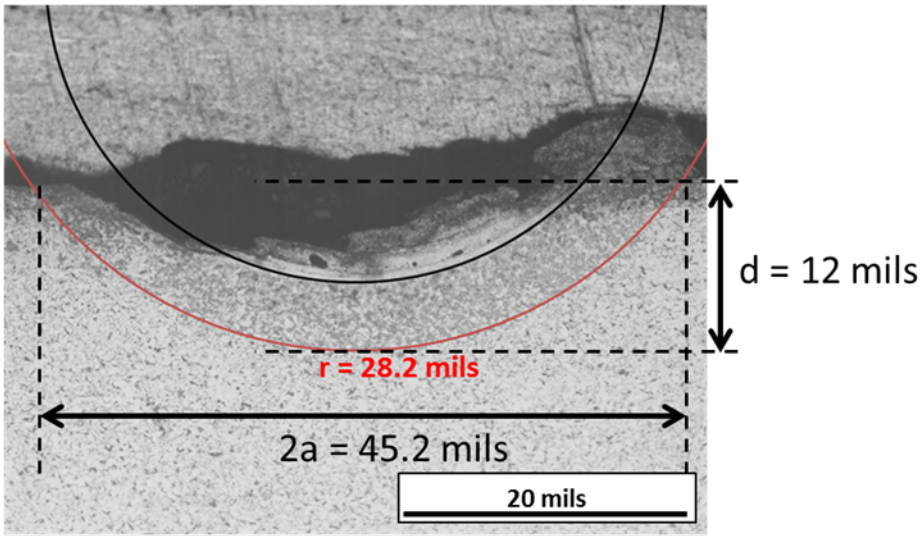

Figure 4-13. Measurement used to estimate K_t of the plasma notch.

5. Mechanical Characterization

Standards for weathering steels are outlined based on the direct application of a member. For example, Specification A588/A588M applies to Grade 50W and outlines required compositional ranges and tensile properties, while Specification A6/A6M applies to several grades and outlines acceptable processing techniques and the resulting microstructures and mechanical properties required for the application.[4] These standards, along with the American Association of State Highway and Transportation Officials (AASHTO) Guidelines [6], must be met for each heat (or each member for fracture-critical members) in order to be put into service. Currently, there are no tests performed in industry to evaluate the fatigue properties of a particular heat because these properties are assumed to be adequate based on the required values for impact toughness and yield strength according to ASTM A709/A709M.[3] AASHTO *Load and Resistance Factor Design (LRFD): Bridge Design Specifications* does outline appropriate fatigue design categories for bridges (as seen in Figure 5-1 [47]). These include Categories A-E', which outline the stress range and fatigue limits required for a given member, where Category A has the highest minimum stress range of approximately 29 ksi (200 MPa) and Category E' has the lowest stress range of approximately 3 ksi (20 MPa). The fatigue limit is reached when a specimen does not fail after 10,000,000 (or 10^7) cycles, at which time the test is stopped.

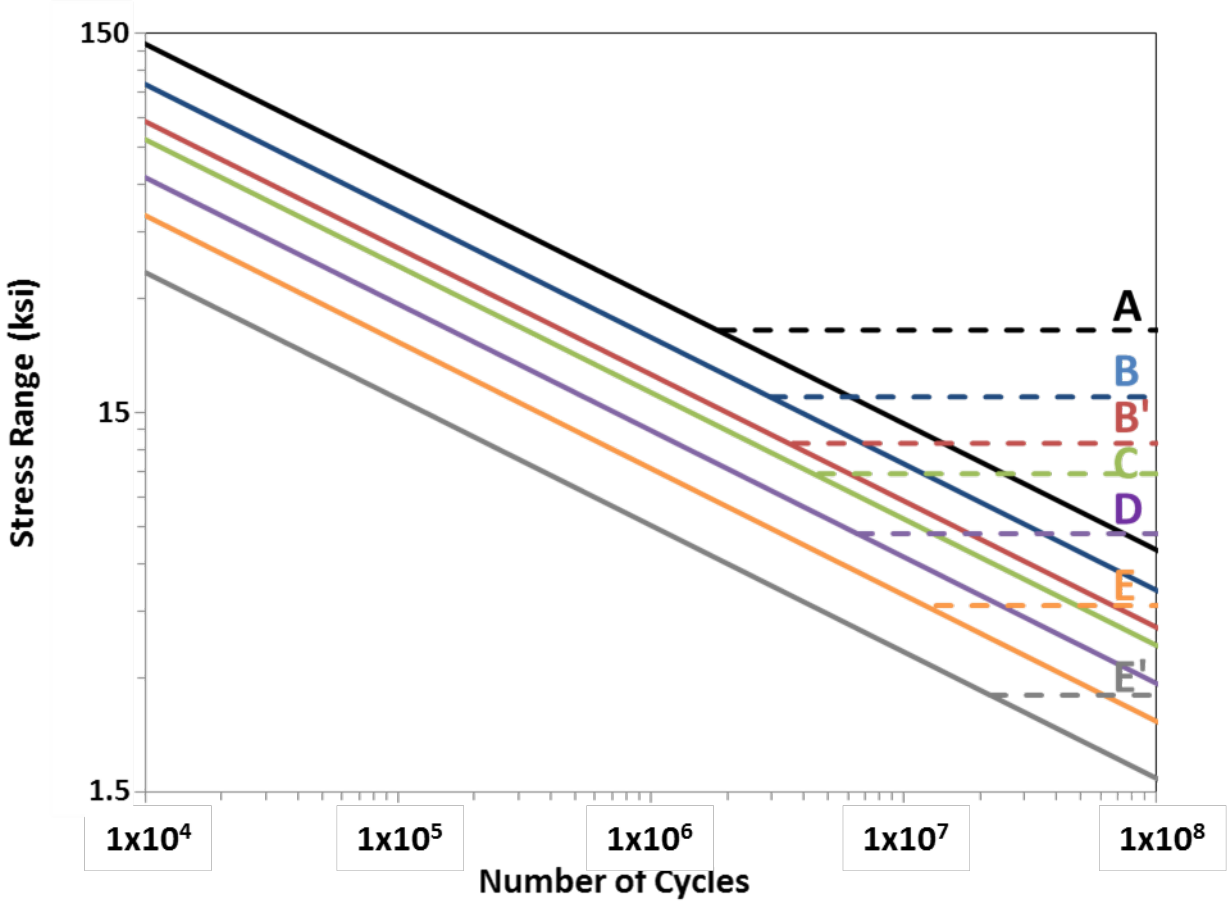

Figure 5-1. AASHTO Fatigue Requirements(Adapted from R.J. Dexter[47]).

5.1 Sample Preparation

5.1.1 Tensile Specimen Preparation

Four tensile bars were fabricated by wire EDM with dimensions outlined by ASTM Standard E8/E8M-09 for a plate of ¼" thickness.[48] The schematic in Figure 5-2 displays the general specimen geometry. All of the tensile samples were cut from the unmarked plate and one of the specimens was polished to a mirror finish using SiC paper and an alumina slurry (240, 320, 400, 600, 1200 grit paper and 1 μm slurry) and the other three specimens were tested in the as-received condition from Tampa Tank. The purpose of polishing one of the samples was to elucidate the effect of surface roughness on the tensile properties of 50W grade steel. The tests were conducted on an Instron 5582 (photographed in Figure 5-3) in displacement control at a crosshead speed of 1.5% of the gauge length per minute. A laser extensometer was used to measure strain.

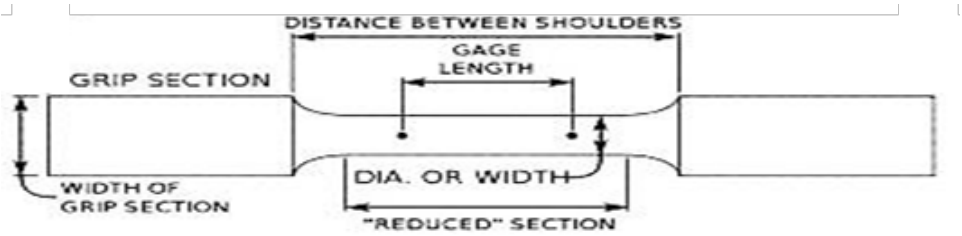

Figure 5-2. Schematic of tensile geometry of ASTM Standard E8/E8M – 09.[48]

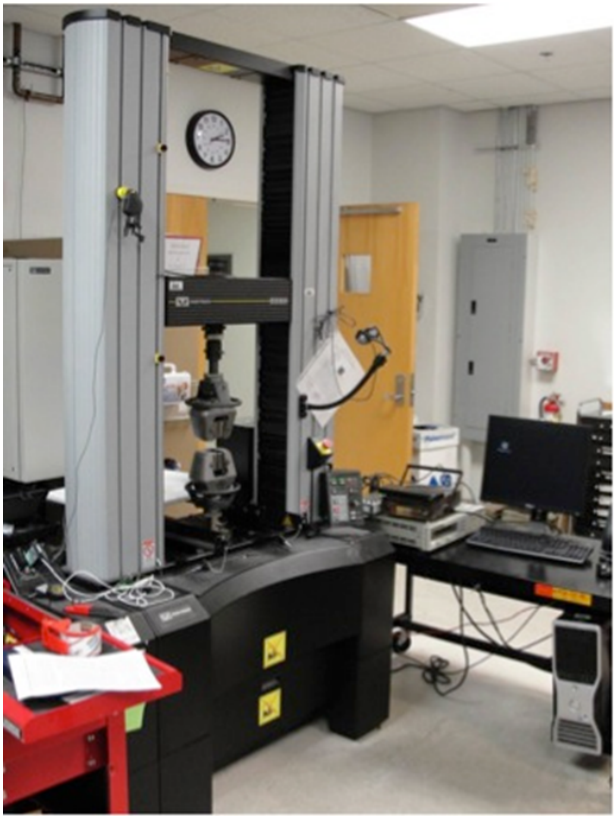

Figure 5-3. Instron 5582 load frame.

5.1.2 Fatigue Specimen Preparation

Twenty four fatigue bars from each condition, unmarked, plasma scribed and laser scribed, were fabricated by wire EDM with dimensions consistent with the Kb-bar geometry (Figure 5-4) used for evaluating the effect of surface flaws on fatigue life.[49, 50] This geometry was chosen due to the scribed

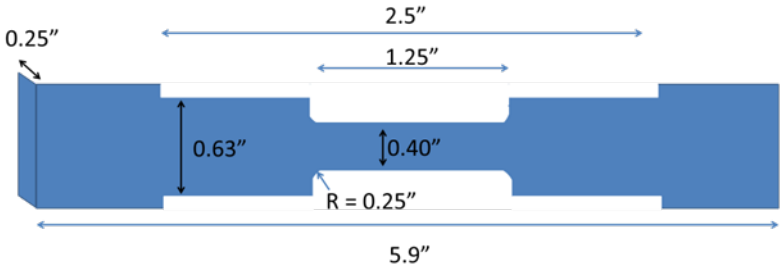

Figure 5-4. Schematic of the fatigue specimen with a Kb-bar geometry and thickness of 0.25"

'notches' not conforming to standard notch sizes for fatigue property evaluation. Conventionally, the notches are a significant fraction of the total thickness of the specimen, on the order of ~0.2 – 0.5, whereas the markings in this study are a maximum of ~0.05 of the total thickness. The fatigue tests were conducted on an MTS 470 servo-hydraulic load frame with and hydraulic grips (photographed in Figure 5-5) in load control at stress ranges of 32.6, 43.1, 45.7, 47 and 48.3 ksi (225, 297, 315, 324 and 333 MPa) with R = 0.1 and frequency of 40 Hz. Four samples were run per stress range. Runout is assumed when the sample undergoes 10^7 cycles. A single cycle is complete once a full sine wave runs to completion, from the median load, up to the maximum load, down to the minimum load and then back to the median load. Stress range versus number of cycles curves (S-N curves) were generated for each marking condition and the unmarked material. These results were compared with the minimum fatigue property requirements outlined by AASHTO.[6]

Figure 5-5. MTS 470 with hydraulic grips.

5.1.3 Fractography

Fractographic specimen preparation required cutting the fracture surface from the gauge of the bar using a slow speed diamond wafering saw while covering the fracture surface to protect it from cutting oil contamination. The fracture surfaces were viewed in an FEI XL40 field emission scanning electron microscope (SEM) in secondary mode. During SEM analysis, energy dispersive spectroscopy (EDS) was conducted on the fracture surface using a Gatan EDAX detector to determine if there was a compositional variation at the initiation site.

5.2 Tensile Testing

Tensile testing results for a polished and an as-received sample are shown in Figure 5-6. These tests were undertaken to confirm that the material conformed to the required minimum properties outlined by ASTM standards and AASHTO guidelines.[3, 4, 6, 48] Additionally, testing conducted on the as-received samples (one representative sample is shown as the red curve in Figure 5-6) were compared to the tensile properties of the polished sample (blue curve in Figure 5-6) that had the weathering layer and areas potentially affected by the machining removed to determine if the surface roughness affected the mechanical properties, principally yield and ultimate tensile strengths of this 50W steel. The yield strength for the tests ranged from 58-60 ksi (400-415 MPa), which exceeds the 50 ksi (345 MPa) required by the standards. The polished sample did not result in a measureable difference when compared to the behavior of the as-received samples.

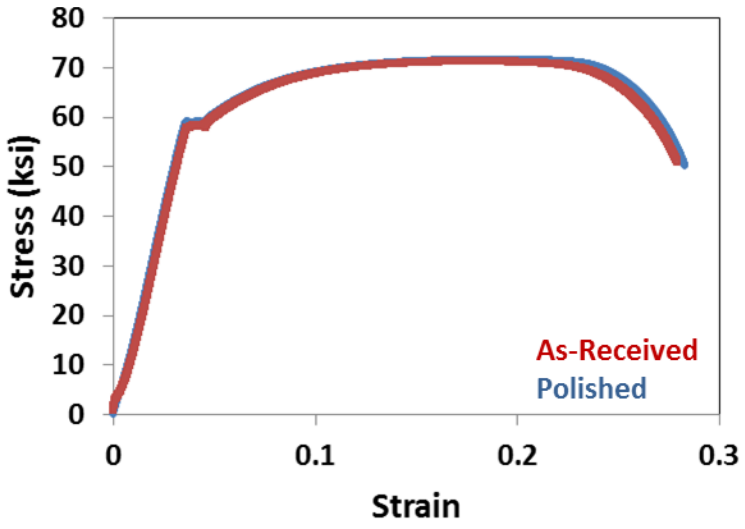

Figure 5-6. Representative stress-strain curves for as-received and polished 50W weathering steel.

5.3 Fatigue Testing

Results for fatigue testing conducted on the unmarked material exceed the minimum required fatigue life for AASHTO Category A. Fatigue results for the unmarked samples are displayed overlaid on the AASHTO fatigue plot in Figure 5-7, and the data are provided in Table A-1 in Appendix A. Photographs of plasma and laser scribed fatigue specimens are shown in Figure 5-8. Figure 5-9 and 5-10 are the results for the plasma and laser notched samples, respectively, and both show sufficient fatigue life required for Category A, as well. These data are provided in Table A-2 in Appendix A. Figure 5-11 shows the data for all three conditions on the same plot, and the scatter in the data resulting from the two marked conditions lies within the scatter of the unmarked material. For the highest stress range of 48.3 ksi (333 MPa), the average cycles to failure and standard deviations are 459,814 ± 85,314, 643,632 ± 82,519, and 480,360 ± 85,079 for the baseline, laser, and plasma samples, respectively. This is a positive result for future implementation of these marking techniques in the production line, but more statistically significant

fatigue testing must be conducted to ensure a high level of confidence and reliability for these fracture-critical member materials.

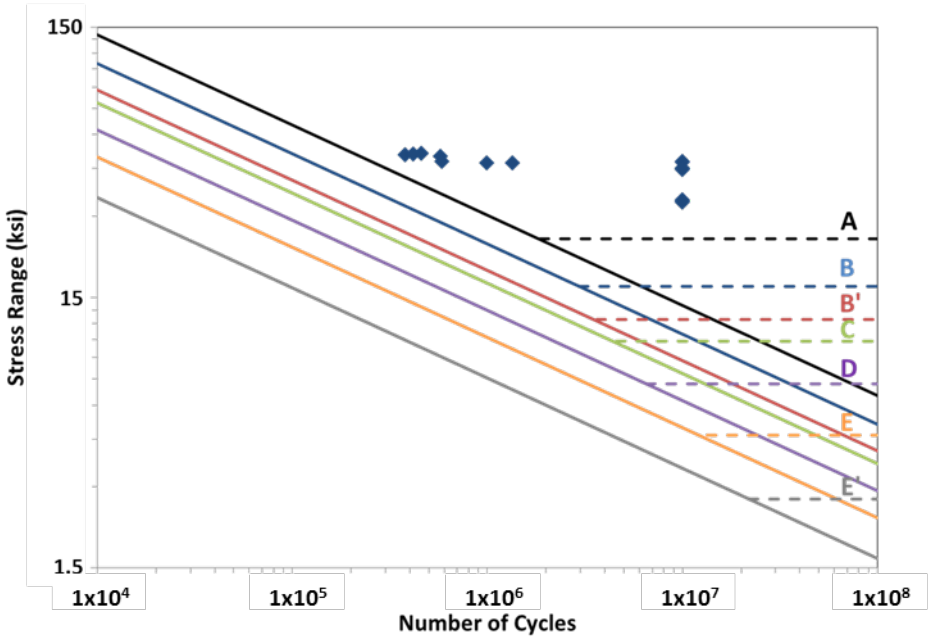

Figure 5-7. S-N curve for unmarked 50W steel.

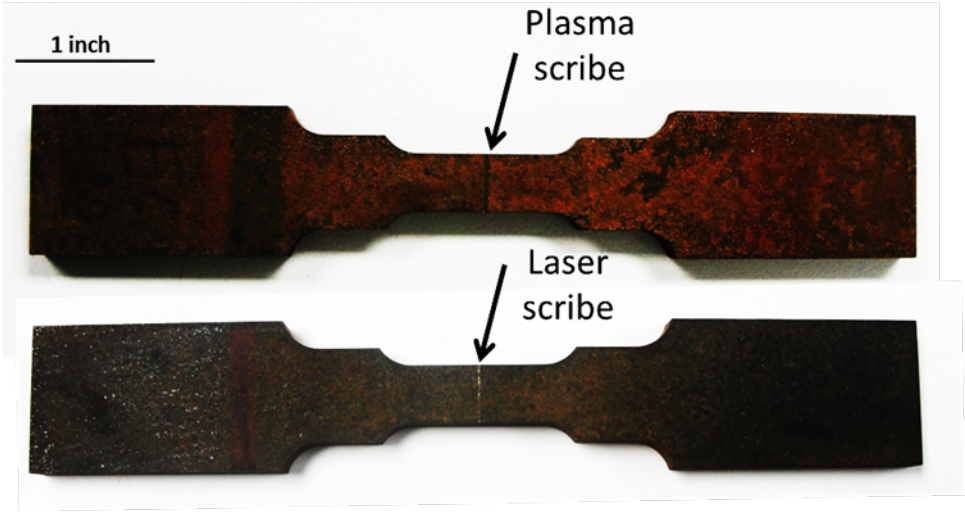

Figure 5-8. Plasma- scribed (top) and laser-scribed (bottom) fatigue specimens.

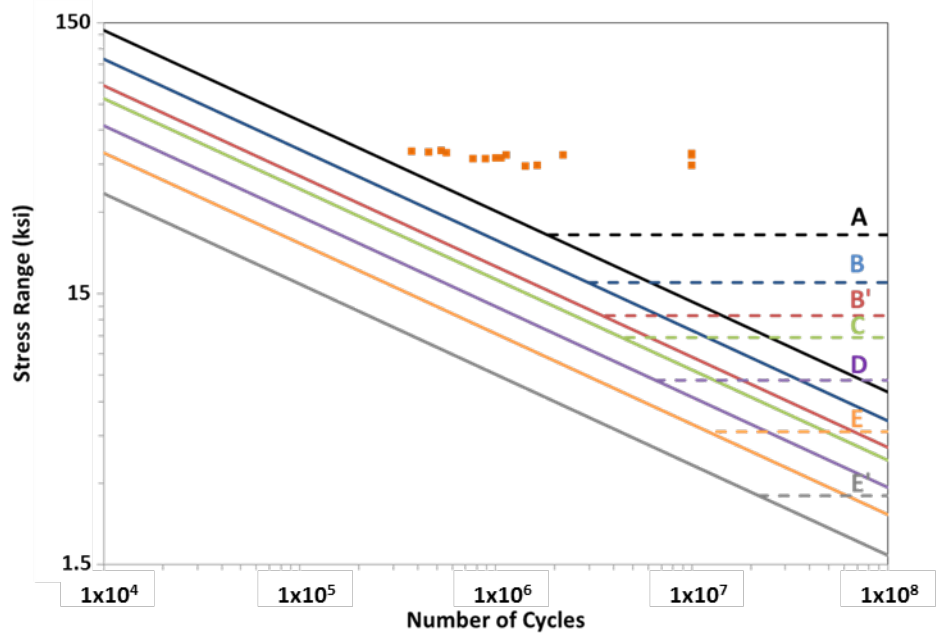

Figure 5-9. S-N curve for plasma-scribed 50W steel.

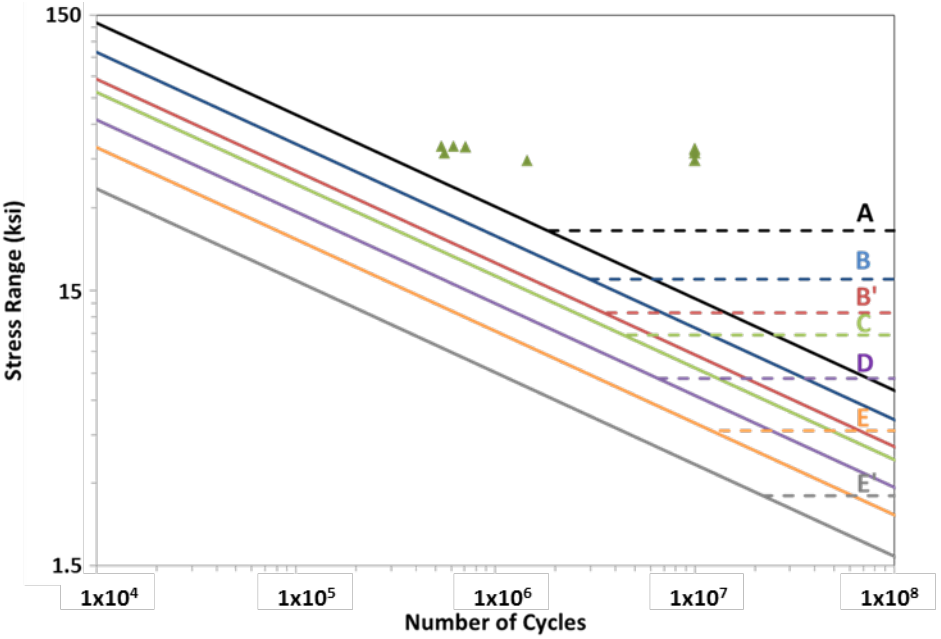

Figure 5-10. S-N curve for laser-scribed 50W steel.

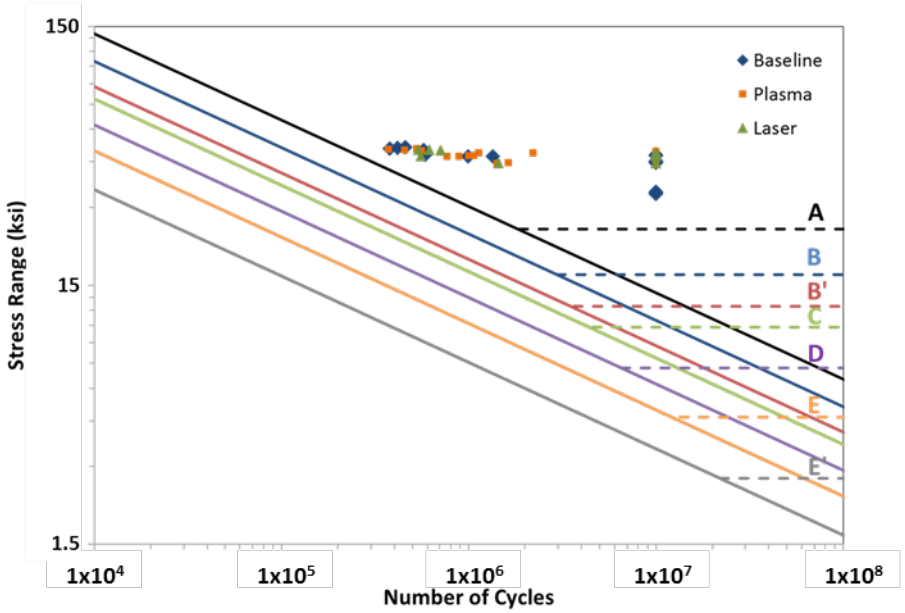

Figure 5-11. S-N curves with all three conditions overlaid.

5.4 Fractography

Despite the presence of plasma and laser scribed notches, fatigue cracks generally formed near the shoulder of the fatigue specimens (Figure 5-12 top). None of the laser scribed notches resulted in fracture initiation at the notch and only two, both tested at a stress range of 48.3 ksi, of the 16 tested plasma notched samples initiated at the notch (Figure 5-12 bottom). The samples shown in Figure 5-12 had fatigue lives of 5.31×10^5 cycles (top) and 5.64×10^5 cycles (bottom). Microscopic analysis conducted on

Figure 5-12. Fatigue specimen that fractured (top) near the shoulder and (bottom) at the plasma notch.

the fracture surfaces of samples that failed near the shoulder of the sample (Figure 5-13) showed that the crack initiated at the surface of the sample and propagated in a relatively planar manner until unstable crack growth (or overload) ensued, resulting in a large region of microvoid coalescence (Figure 5-13a), indicating shearing and ductile fracture. SEM imaging shows two initiation sites (Figure 5-13b) and at higher magnification the size of the initiation site is outlined with a dotted line in Figure 5-13c. The initiation appears to be a result of a surface flaw likely due to an uneven weathered oxide layer. The

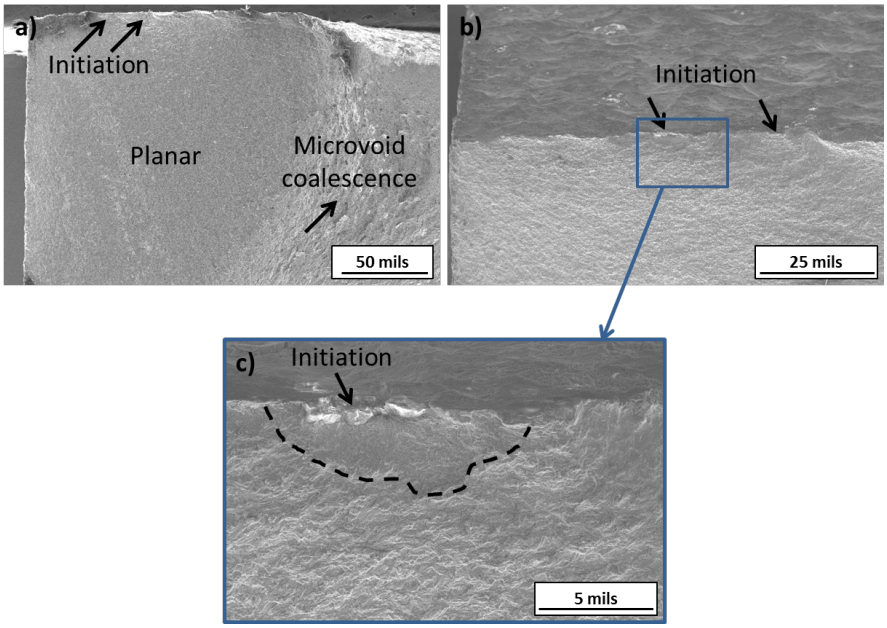

Figure 5-13. SEM micrographs of a) the macroscopic fracture surface, b) initiation sites and c) an outlined initiation site for a 50W steel specimen that fractured near the shoulder.

fracture surfaces were macroscopically similar for all samples when fracture initiated at the shoulder, however, the samples where fracture initiated at the notch had unique features associated with the initiation site and the crack propagation in the heat-affected zone near the notch. Figure 5-14a shows a low magnification view of a specimen that fractured at the plasma notch. Higher magnification of the initiation site, shown in Figure 5-14b and 5-14c, reveals a smoother, more faceted initiation site compared with the initiation shown in Figure 5-13c. The EDS map taken of the region (Figure 5-14d) shows

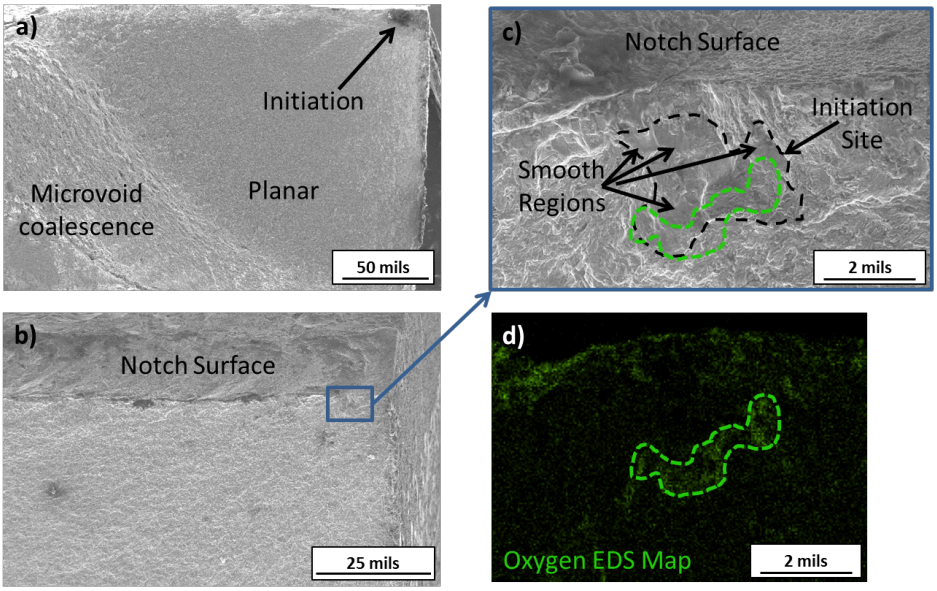

Figure 5-14. SEM micrographs of a) the macroscopic fracture surface, b) initiation sites, c) an outlined initiation site and d) an EDS map of oxygen for plasma scribed 50W steel that fractured at the scribed marking.

evidence of oxygen at the initiation site, suggesting the presence of an oxide inclusion. The smooth, faceted areas of the fracture initiation site (Figure 5-14c) are indicative of transgranular cleavage that is commonly observed at the site of initiation of fracture in fatigue.[51] As the fatigue crack propagates, the planar and sheared regions away from the notch are topographically similar to the crack propagation in the samples where fracture initiated near the shoulder, however, propagation in the immediate vicinity of the notch results in a thin region of intergranular fracture (Figure 5-15). This intergranular fracture corresponds with the 'Inner' region, and is shown again here in Figure 5-15a. These exposed grains (Figure 5-15b and 5-15c) are in the same region as the initiation site (Figure 5-14) and likely represent the same microstructure present in the 'Inner' region. Fracture initiated internally in the 'Inner' region in a transgranular manner, and then propagated through the 'Inner' region adjacent to the notch intergranularly. Despite the apparent differences in the sources and topography of the notch and shoulder crack initiation, the size of the initiation sites are similar (approximately 2.75 mils) and the fatigue behavior of the specimen fall in the same range of scatter for the number of cycles for the fatigue tests. Without further fatigue testing, it is difficult to statistically quantify the risk of failure for the marked specimens. While this study shows no measureable differences, a more rigorous, statistical significant study will be necessary to evaluate the risk over a larger sample range. Work is ongoing to explore a larger population of samples.

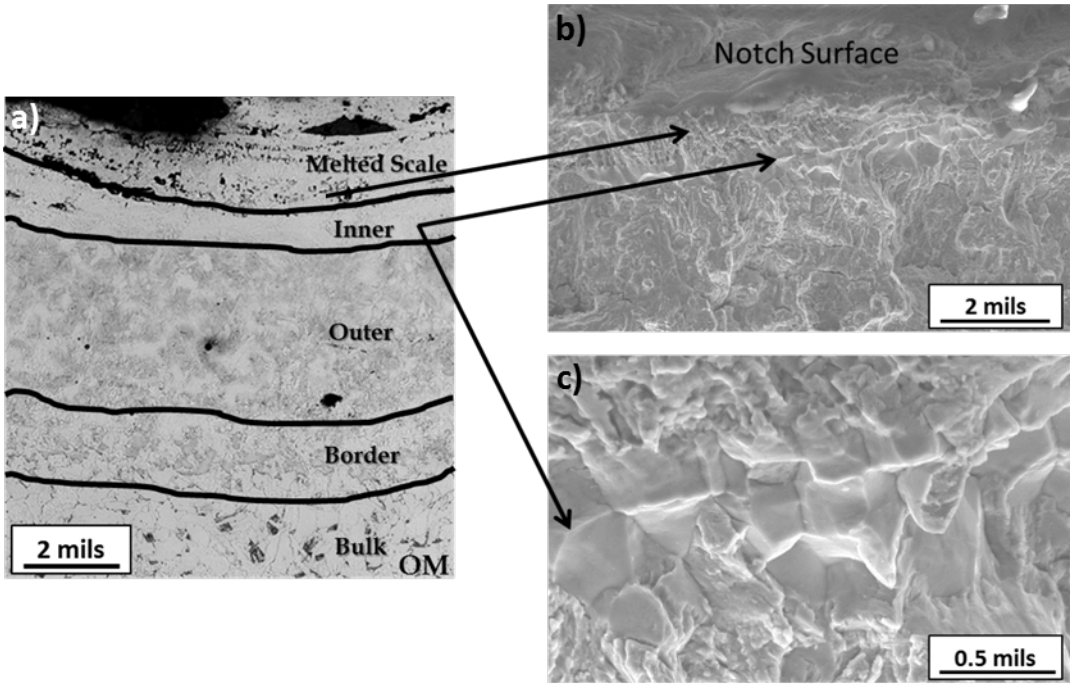

Figure 5-15. An optical micrograph of a) the profile of the HAZ caused by the plasma scribe and SEM micrographs of b) the fracture surface near the notch surface associated with the crack propagation showing c) intergranular fracture in the 'Inner' region.

6. Conclusion

The ¼" 50W steel plates acquired from Veritas Steel conformed to ASTM and AASHTO standards for grain size and composition. The plates were marked with mechanical, plasma and laser scribes. Both plasma and laser scribes were sufficient in making a mark that was visible after sandblasting and weathering. However, mechanical milling was insufficient and shallow at the condition employed for this study. The plasma scribe was the fastest technique and had the most noticeable marking, though it resulted in a noticeable HAZ compared to the other techniques. Vickers microhardness testing on the HAZ of the plasma notch showed increasing hardness from the bulk to the notch surface. A stress concentration factor of 1.7 was calculated for the plasma notch. While the maximum stress at the notch root is approximately 1.7X that of the bulk, the 3-fold increase in hardness may impart enhanced fatigue strength in the immediate vicinity of the notch.

The tensile strength of these specimens was confirmed to exceed the minimum requirements outlined by ASTM Standards and AASHTO requirements. All specimens, marked and unmarked, showed sufficient fatigue life in accordance with AASHTO guidelines for Category A. The plasma scribed notch, which provided in the deepest notch with a noticeable heat-affected zone (HAZ), did not result in measureable degradation of fatigue life from the generated S-N curve. Fractography conducted on the samples which fractured near the shoulder of the fatigue specimen showed typical initiation and propagation for a high-strength low-alloy steel. None of the laser scribed samples fractured on the scribed marked during fatigue testing and only 2 of the 16 plasma scribed samples had fracture initiation occurring at the mark. Observation of the fracture which initiated near the plasma scribed mark showed a transgranular initiation site in the 'Inner' region of the HAZ which then propagated through this region in an intergranular manner, but ultimately followed a similar path through the bulk of the specimens where fracture initiated near the shoulder.

References

1. Pickering, F.B., *Physical Metallurgy and the Design of Steels*. Materials science series. 1978, London: Applied Science Publishers.
2. ASM International 2013. *Properties and selection-- irons, steels, and high-performance alloys*. Materials Park, OH: ASM International.
3. ASTM, *Standard Specification for Structural Steel for Bridges*. Vol. 01.04. 2011, West Conshohocken: ASTM International.
4. ASTM, *Standard Specification for General Requirements for Rolled Structural Steel Bars, Plates, Shapes, and Sheet Piling*. Vol. 01.04. 2011, West Conshohocken: ASTM International.
5. ASTM, *Standard Specification for Sampling Procedure for Impact Testing of Structural Steel*. Vol. 01.04. 2012, West Conshohocken: ASTM International.
6. AASHTO, *LRFD bridge design specifications*. 2nd ed. 1998, Washington, DC.
7. Sherman, R., *Quality Engineer*, M.S. Kesler, Editor. 2013.
8. Faulkner, L., Automating Layout in Steel Fabrication. 2011: *Modern Steel Construction*.
9. ASM International. 2001, *Alloying: Understanding the Basics*, in *High-Strength Low-Alloy Steels*. ASM International.
10. Albrecht, P. and A. Lenwari, Fatigue Strength of Weathered A588 Steel Beams. *Journal of Bridge Engineering*, 2009. **14**(6): p. 436-443.
11. Kulicki, J.M. Steel Bridges for the 21st Century, *Advanced Technology in Structural Engineering*, 2004.
12. Wright, W.J., *Steel Bridge Design Handbook: Bridge Steels and Their Mechanical Properties*. 2012.
13. Bae, Y.H., et al., Effects of Austenite Conditioning on Austenite/Ferrite Phase Transformation of HSLA Steel. *Materials Transactions*, 2004. **45**(1): p. 137-142.
14. Cuddy, L.J., Microstructures Developed During Thermomechanical Treatment of HSLA Steels. *Metallurgical Transactions a-Physical Metallurgy and Materials Science*, 1981. **12**(7): p. 1313-1320.
15. Cuddy, L.J. and J.C. Raley, Austenite Grain Coarsening in Microalloyed Steels. *Metallurgical Transactions a-Physical Metallurgy and Materials Science*, 1983. **14**(10): p. 1989-1995.
16. Cuddy, L.J., Grain-Refinement of NB Steels by Control of Recrystallization During Hot-Rolling. *Metallurgical Transactions A-Physical Metallurgy and Materials Science*, 1984. **15**(1): p. 87-98.
17. Pickering, F.B. and B. Garbarz, Strengthening in Pearlite Formed From Thermomechanically Processed Austenite in Vanadium Steels and Implications For Toughness. *Materials Science and Technology*, 1989. **5**(3): p. 227-237.
18. Irvine, K.J., et al., Controlled Rolling of Structural Steels. *Journal of the Iron and Steel Institute*, 1970. **208**: p. 717-&.
19. Kayser, C.R., J.A. Swanson, and D.G. Linzell, Characterization of Material Properties of HPS-485W (70W) TMCP For Bridge Girder Applications. *Journal of Bridge Engineering*, 2006. **11**(1): p. 99-108.
20. Chen, H.T., G.Y. Grondin, and R.G. Driver, Characterization of Fatigue Properties of ASTM A709 High Performance Steel. *Journal of Constructional Steel Research*, 2007. **63**(6): p. 838-848.
21. De, A., M. Manohar, and W. Heitmann, Processing Alternatives for Optimized Strength and Toughness Balance of ASTM A709 PS 70W Composition, in *Materials Science & Technology 2007 Conference and Exhibition*. 2007: Detroit, Michigan.
22. Chen, H., G.Y. Grondin, and R.G. Driver, Fatigue Resistance of High Performance Steel., in *6th Intl. Conference on Short and Medium Span Bridges*. 2002: Vancouver, Canada.
23. Illescas, S., et al., Study of the Mechanical Properties of Low Carbon Content HSLA Steels. *Revista De Metalurgia*, 2009. **45**(6): p. 424-431.

24. Wright, W.J., et al., Fracture Resistance of Modern Bridge Steels, in *Advanced Technology in Structural Engineering*. 2000. p. 1-9.
25. Seradj, H. Design and Fabrication of the Sylvan Overcrossing HPS 70W Box Girder Bridge. in *Federal Highway Administration (FHWA) Steel Bridge Conf.* 2004. San Antonio, TX.
26. Albrecht, P. and C. Shabshab, Fatigue Strength of Weathered Rolled Beam Made of A588 Steel. *J. Mater. Civ. Eng.*, 1994. **6**(3): p. 407-428.
27. Bennett, C.R., J.A. Swanson, and D.G. Linzell, Fatigue resistance of HPS-485W (70W) Continuous Plate With Punched Holes. *Journal of Bridge Engineering*, 2007. **12**(1): p. 98-104.
28. Swanson, J.A., et al., Verification of Performance and Design Criteria for High Performance Steel Bridges. 2006, University of Cincinnati Department of Civil & Environmental Engineering.
29. Boyer, H., *Atlas of Fatigue Curves*. 1986, ASM.
30. Sánchez, L., F. Gutiérrez-Solana, and D. Pesquera, Fatigue Behaviour of Punched Structural Plates. *Engineering Failure Analysis*, 2004. **11**(5): p. 751-764.
31. Neuber, H., Theory of Stress Concentration for Shear-Strained Prismatical Bodies With Arbitrary Nonlinear Stress-Strain Law. *Journal of Applied Mechanics*, 1961. **28**(4): p. 544-550.
32. Sherman, A.M., Fatigue Properties of High Srength Low Alloy-Steels. *Metallurgical Transactions*, 1975. **A 6**(5): p. 1035-1040.
33. Peddinghaus. 2012; Available from: http://www.peddinghaus.com/.
34. Voortman. 2014; Available from: http://www.voortman.net/en/.
35. *Controlled Automation*. 2014; Available from http://www.controlledautomation.com/.
36. Chen, Y.T., et al., Microstructure and Mechanical Properties Development in the Simulated Heat-Affected Zone of V Treated HSLA Steels. *Acta Metallurgica Sinica* (English Letters), 2006. **19**(1): p. 57-67.
37. Spies, H.J., Pusch, G., Henkel, C., Robler, K., Fatigue Crack-Propagation in High-Strength Low-Alloy Steels. *Theoretical and Applied Fracture Mechanics*, 1989. **11**(2): p. 121-125.
38. Kim, B.C., Lee, S., Kim, N.J., Lee, D.Y., et al., Microstructure and Local Brittle Zone Phenomena in High-Strength Low-Alloy Steel Welds, *Metallurgical Transactions a-Physical Metallurgy and Materials Science*, 1991. **22**(1): p. 139-149.
39. Tsay, L.W., Li, Y.M., Chen, C., Cheng, S.W., Mechanical properties and fatigue crack growth rate of laser-welded 4130 steel. *International Journal of Fatigue*, 1992. **14**(4): p. 239-247.
40. Shi, Y. and Z. Han, Effect of Weld Thermal Cycle on Microstructure and Fracture Toughness of Simulated Heat-Affected Zone for a 800-MPa Grade High Strength Low Alloy Steel. *Journal of Materials Processing Technology*, 2008. **207**(1–3): p. 30-39.
41. Boardman, B., *Fatigue Resistance of Steels*. ASM Handbook Volume 1, *Properties and Selection: Irons, Steels, and High-Performance Alloys* (ASM International), 1990.
42. ASM International. 2001 *High-Strength Low-Alloy Steels*. Materials Park, OH: ASM International.
43. ASTM, *Standard Test Methods for Determining Average Grain Size*. Vol. 03.01. 2014, West Conshohocken: ASTM International.
44. Tsao, C.H., A. Ching, and S. Okubo, Stress Concentration Factors for Semi-elliptical Notches in Beams Under Pure Bending. *Experimental Mechanics*, 1965. **5**: p. 19A.
45. Ohta, A., Y. Maeda, and N. Suzuki, Effect of Yield Strength on the Basic Fatigue-Strength of Welded-Joints. *Fatigue & Fracture of Engineering Materials & Structures*, 1993. **16**(5): p. 473-479.
46. Pang, J.C., et al., General Relation Between Tensile Strength and Fatigue Strength of Metallic Materials. *Materials Science and Engineering: A*, 2013. **564**(0): p. 331-341.
47. Dexter, R., *Handbook of Structural Engineering*. 2nd ed. 2005: CRC Press.
48. ASTM, *Standard Test Methods for Tension Testing of Metallic Materials*. Vol. 03.01. 2011: ASTM International.

49. Halford, G. and J. Gallagher, *Fatigue and Fracture Mechanics: 31st Volume*. 2000: ASTM International.
50. Nicholas, T., Chapter 8 - HCF Design Considerations, in *High Cycle Fatigue*, T. Nicholas, Editor. 2006, Elsevier Science Ltd: Oxford. p. 379-471.
51. Meyers, M. and K. Chawla, *Mechanical Behavior of Materials*. 2002, Upper Saddle River, New Jersey: Prentice Hall, Inc.

Appendix A: Fatigue Data

Table A-1. Fatigue data for unmarked samples.

Stress Range in ksi (MPa)	Number of Cycles
	Baseline
48.3 (333)	$3.80x10^5$
	$4.61x10^5$
	$4.19x10^5$
	$5.78x10^5$
45.7 (315)	$5.85x10^5$
	$1.35x10^6$
	$1.0x10^7$
	$1.0x10^7$
43.1 (297)	$1.0x10^7$
	$1.0x10^7$
	$1.0x10^7$
	$1.0x10^7$
32.6 (225)	$1.0x10^7$
	$1.0x10^7$
	$1.0x10^7$
	$1.0x10^7$

Table A-2. Fatigue data for laser and plasma scribed samples. The values highlighted in red and marked with an asterisk (*) represent the two samples that broke at the scribe mark.

Stress Range in ksi (MPa)	Number of Cycles	
	Laser	**Plasma**
48.3 (333)	5.37×10^5	5.31×10^5
	7.08×10^5	***3.73×10^5**
	7.09×10^5	4.54×10^5
	6.20×10^5	***5.64×10^5**
47 (324)	1.0×10^7	2.22×10^6
	1.0×10^7	1.0×10^7
	---	1.14×10^5
	---	1.0×10^7
45.7 (315)	1.0×10^7	1.0×10^6
	1.0×10^7	7.69×10^5
	5.54×10^5	8.86×10^5
	1.0×10^7	1.07×10^6
43.1 (297)	1.0×10^7	1.0×10^7
	1.0×10^7	1.0×10^7
	1.45×10^6	1.0×10^7
	1.0×10^7	1.63×10^6